

High density symmetry energy: A key to the solution of the hyperon puzzle

JUN-TING YE ¹, RUI WANG ², SI-PEI WANG ¹ AND LIE-WEN CHEN ¹

¹*School of Physics and Astronomy, Shanghai Key Laboratory for Particle Physics and Cosmology, and Key Laboratory for Particle Astrophysics and Cosmology (MOE), Shanghai Jiao Tong University, Shanghai 200240, China*

²*Istituto Nazionale di Fisica Nucleare (INFN), Sezione di Catania, I-95123 Catania, Italy*

ABSTRACT

The recently developed nuclear effective interaction based on the so-called N3LO Skyrme pseudopotential is extended to include the hyperon-nucleon and hyperon-hyperon interactions by assuming the similar density, momentum, and isospin dependence as for the nucleon-nucleon interaction. The parameters in these interactions are determined from either experimental information if any or chiral effective field theory or lattice QCD calculations of the hyperon potentials in nuclear matter around nuclear saturation density ρ_0 . We find that varying the high density behavior of the symmetry energy $E_{\text{sym}}(\rho)$ can significantly change the critical density for hyperon appearance in the neutron stars and thus the maximum mass M_{TOV} of static hyperon stars. In particular, a symmetry energy which is soft around $2 - 3\rho_0$ but stiff above about $4\rho_0$, can lead to $M_{\text{TOV}} \gtrsim 2M_{\odot}$ for hyperon stars and simultaneously be compatible with (1) the constraints on the equation of state of symmetric nuclear matter at suprasaturation densities obtained from flow data in heavy-ion collisions; (2) the microscopic calculations of the equation of state for pure neutron matter; (3) the star tidal deformability extracted from gravitational wave signal GW170817; (4) the mass-radius relations of PSR J0030+0451, PSR J0740+6620 and PSR J0437-4715 measured from NICER; (5) the observation of the unusually low mass and small radius in the central compact object of HESS J1731-347. Furthermore, the sound speed squared of the hyperon star matter naturally displays a strong peak structure around baryon density of $3 - 4\rho_0$, consistent with the model-independent analysis on the multimessenger data. Our results suggest that the high density symmetry energy could be a key to the solution of the hyperon puzzle in neutron star physics.

Keywords: dense matter — equation of state — stars: neutron — stars: interiors

1. INTRODUCTION

In the dense cores of neutron stars (NSs), the chemical potentials of nucleons may reach sufficiently high levels to enable their β decay into hyperons. Neutron stars with such interiors, consisting not only of nucleons and leptons but also of hyperons, are referred to as hyperon stars (HSs). The presence of hyperons releases Fermi pressure and renders the equation of state (EOS) of NS matter softer, consequently resulting in that the maximum mass of NSs might not align with astrophysical observations of massive NSs with mass larger than about $2M_{\odot}$ (Antoniadis et al. 2013; Cromartie et al.

2019; Fonseca et al. 2021). This phenomenon is commonly known as “hyperon puzzle” (Chatterjee & Vidaña 2016; Vidaña 2018; Tolos & Fabbietti 2020; Bombaci 2021; Burgio et al. 2021; Vidaña 2022; Tolos 2024).

The study of the hyperon puzzle is closely linked to the EOS of dense nuclear matter, which reflects the fundamental properties of effective nuclear interactions. Experimentally, analyses on the data from the giant monopole resonance in finite nuclei (Youngblood et al. 1999; Li et al. 2007, 2023; Shlomo et al. 2006; Garg & Colò 2018) as well as the measurements of collective flow (Danielewicz et al. 2002; Le Fèvre et al. 2016) and kaon production (Aichelin & Ko 1985; Fuchs et al. 2001; Hartnack et al. 2006; Fuchs 2006) in high energy heavy-ion collisions (HICs) have already provided valuable constraints on the EOS of symmetric nuclear matter (SNM) from nuclear saturation density ρ_0 to suprasaturation

density of about $5\rho_0$. On the other hand, for the isospin-dependent part of nuclear matter EOS, characterized by the so-called nuclear symmetry energy $E_{\text{sym}}(\rho)$, its suprasaturation density behavior is still among the most uncertain properties of nuclear matter (Li et al. 2008; Sorensen et al. 2024), although the symmetry energy at densities below and around ρ_0 has been reasonably well-constrained through nuclear structure probes (Chen et al. 2005a; Centelles et al. 2009; Chen et al. 2010; Agrawal et al. 2012; Zhang & Chen 2013; Brown 2013; Roca-Maza et al. 2013; Zhang & Chen 2014; Danielewicz & Lee 2014; Danielewicz et al. 2017; Xu et al. 2020; Qiu et al. 2024) and observables in HICs at energies less than about 100 MeV/nucleon (Chen et al. 2005b; Li & Chen 2005; Kowalski et al. 2007; Shetty et al. 2007; Tsang et al. 2009; Wada et al. 2012; Morfouace et al. 2019; Zhang et al. 2020). In recent years, significant progress has been made to constrain the high density behavior of the symmetry energy by using the multi-messenger data, especially the gravitational wave observation in binary neutron star merger as well as the simultaneous determination of the mass and radius of NSs by NICER, but the uncertainty of the constraints is still very large (Fiorella Burgio & Fantina 2018; Zhang & Li 2019; Zhou et al. 2019; Zhou & Chen 2019; Li et al. 2021; Krastev 2022; Yue et al. 2022; Koehn et al. 2024). Besides adhering to the constraints imposed by terrestrial experiments and astrophysical observations, it is interesting to mention that the systematics of the density dependence of the symmetry energy based on a large samples of theoretical models can also provide estimate on the suprasaturation density behavior of the symmetry energy from their precise knowledge around saturation density (Chen 2011, 2015).

While extensive research has focused on understanding the nucleon-nucleon (NN) interaction, comparatively less attention has been given to investigating the hyperon-nucleon (YN) and the hyperon-hyperon (YY) interactions. Experimentally, the available scattering data includes several hundred measurements for ΛN (Alexander et al. 1968; Sechi-Zorn et al. 1968; Kadyk et al. 1971) and ΣN (Engelmann et al. 1966; Eisele et al. 1971), but there is a scarcity of information regarding ΞN . Furthermore, over forty single Λ -hypernuclei as well as some double Λ (Danysz et al. 1963; Prowse 1966; Takahashi et al. 2001) and single Ξ (Vidaña 2018) hypernuclei have been discovered. However, experimental data for YY interactions remains missing. Theoretically, various models have been developed by extending the nucleonic interaction to describe hyperonic interactions. These models can be roughly classified into phenomenological and microscopic ap-

proaches. Phenomenological methods, such as non-relativistic Skyrme interaction (Skyrme 1959) and relativistic mean-field (RMF) theory (Walecka 1985; Serot & Walecka 1997), are widely employed in this context. The microscopic calculations involve starting with realistic interactions and constructing them using meson-exchange theory (Holzenkamp et al. 1989; Stoks & Rijken 1999; Rijken et al. 1999), quark models (Fujiwara et al. 2007), chiral effective field theory (χ EFT) (Weinberg 1990; Polinder et al. 2006; Haidenbauer et al. 2013), and Lattice Quantum Chromodynamics (LQCD) (Ishii et al. 2007; Beane et al. 2012; Nemura et al. 2018). Many-body problems are then solved through techniques like the Brueckner-Hartree-Fock (BHF) approximation (Baldo et al. 2000; Vidana et al. 2000).

Currently, several potential solutions to the hyperon puzzle have been proposed (Vidaña 2018; Tolos 2024). The primary objective of these approaches is to enhance the stiffness of the hyperonic matter EOS in order to ensure that the maximum mass of HSs remains sufficiently large. Strengthening YN and YY interactions (Bednarek et al. 2012; Weissenborn et al. 2012; Jiang et al. 2012; Gomes et al. 2015; Maslov et al. 2015; Li et al. 2018a; Sun et al. 2023; Wei et al. 2024) or introducing more repulsive three-body forces (Tsubakihara & Ohnishi 2013; Lonardonì et al. 2015; Logoteta et al. 2019; Gerstung et al. 2020) involving hyperons could effectively stiffen the EOS for hyperonic matter. Additionally, it is also plausible to consider a phase transition to deconfined quark matter with stiff EOS (Ozel et al. 2010; Weissenborn et al. 2011; Zdunik & Haensel 2013) occurring prior to the appearance of hyperons. Furthermore, there is consideration regarding the inclusion of Δ baryons (Drago et al. 2014; Li et al. 2018b) or kaon condensate (Glendenning & Schaffner-Bielich 1998; Muto 2008), which may delay the onset of hyperons until higher densities are reached. Moreover, accounting for momentum dependent in-medium potentials for hyperons (Chorozidou & Gaitanos 2024) is of significant importance as well. Some unconventional methods such as modifying gravity (Astashenok et al. 2014) have even been proposed. For the moment, nevertheless, resolution to the hyperon puzzle remains elusive.

In this work, we propose that the high density symmetry energy could be a key to solve the hyperon puzzle. We first extend the recently developed N3LO Skyrme pseudopotential (Wang et al. 2018, 2024) to describe the interactions of octet baryons by assuming that the YN and YY interactions have similar density, momentum and isospin dependence as the NN interaction with some scaling parameters. The scaling parameters are then adjusted to fit the single-hyperon potentials in SNM and

pure neutron matter (PNM) obtained from experiments if any, χ EFT (Petschauer et al. 2016) or LQCD (Inoue 2019). By varying the high density behavior of the symmetry energy, we find that the symmetry energy can significantly change the critical density of hyperon appearance in NSs, and a symmetry energy soft at intermediate density but stiff at high density can support a massive HS with mass larger than $2.0M_\odot$ and simultaneously be compatible with current popular constraints from theory, experiments and observations.

We note that a number of studies (Ryu et al. 2011; Cavagnoli et al. 2011; Providencia & Rabhi 2013; Providência et al. 2014; Bizarro et al. 2015; Providência et al. 2018; Choi et al. 2021; Ghosh et al. 2022; Thapa & Sinha 2022; Kumar et al. 2024) have been devoted to exploring the symmetry energy effects on the properties of HSs, essentially via varying the slope parameter L with the high density symmetry energy changed automatically according to the adopted energy density functional. In the present work, we investigate the high density symmetry energy effects through varying independently the higher-order symmetry energy parameters, namely, the curvature parameter K_{sym} and the skewness parameter J_{sym} , while keeping the L parameter unchanged in our energy density functional.

This article is organized as follows. In Section 2, we mainly describe the model and method used in extending the recently developed N3LO Skyrme pseudopotential to include the YN and YY interactions. We then present in Section 3 the results and discussions on how the high density symmetry energy may influence the properties of NSs and HSs. Finally, the conclusion and outlook are given in Section 4.

2. MODEL AND METHOD

2.1. Nuclear matter EOS and its characteristic parameters

The EOS of nuclear matter, which is defined as the binding energy per nucleon, can be expressed as

$$E(\rho, \delta) = E_0(\rho) + E_{\text{sym}}(\rho)\delta^2 + \mathcal{O}(\delta^4), \quad (1)$$

where $\rho = \rho_n + \rho_p$ represents the total nucleon density, which is the sum of the neutron density ρ_n and proton density ρ_p ; $\delta = (\rho_n - \rho_p)/\rho$ denotes the isospin asymmetry; $E_0(\rho) = E(\rho, \delta = 0)$ represents the EOS of SNM; and the symmetry energy $E_{\text{sym}}(\rho)$ can be obtained as

$$E_{\text{sym}}(\rho) = \frac{1}{2!} \left. \frac{\partial^2 E(\rho, \delta)}{\partial \delta^2} \right|_{\delta=0}. \quad (2)$$

Around the saturation density ρ_0 , the $E_0(\rho)$ can be expressed approximately in terms of its incompressibility coefficient K_0 and skewness parameter J_0 as

$$E_0(\rho) = E_0(\rho_0) + \frac{1}{2!} K_0 \chi^2 + \frac{1}{3!} J_0 \chi^3 + \mathcal{O}(\chi^4), \quad (3)$$

where $\chi = (\rho - \rho_0)/(3\rho_0)$ is a dimensionless parameter representing the density deviation from the saturation density ρ_0 . Similarly, by expanding $E_{\text{sym}}(\rho)$ around a reference density ρ_r in terms of its slope parameter $L(\rho_r)$, curvature parameter $K_{\text{sym}}(\rho_r)$ and skewness parameter $J_{\text{sym}}(\rho_r)$, we have

$$E_{\text{sym}}(\rho) = E_{\text{sym}}(\rho_r) + L(\rho_r)\chi_r + \frac{1}{2!} K_{\text{sym}}(\rho_r)\chi_r^2 + \frac{1}{3!} J_{\text{sym}}(\rho_r)\chi_r^3 + \mathcal{O}(\chi_r^4), \quad (4)$$

where χ_r is defined as $\chi_r = (\rho - \rho_r)/(3\rho_r)$. By setting $\rho_r = \rho_0$, one can then obtain the conventional characteristic parameters $L \equiv L(\rho_0)$, $K_{\text{sym}} \equiv K_{\text{sym}}(\rho_0)$ and $J_{\text{sym}} \equiv J_{\text{sym}}(\rho_0)$.

2.2. N3LO Skyrme pseudopotential for baryon octet

We generalize the recently developed extended N3LO Skyrme pseudopotential (Wang et al. 2018, 2024) to include the interactions of octet baryons. When focusing on the spin-averaged quantities as we are interested in here, there only contains the central term $V_{\text{N3LO}}^{\text{C}}$ and the density-dependent term $V_{\text{N1LO}}^{\text{DD}}$ in the extended N3LO Skyrme pseudopotential v_{Sk} for nucleonic interaction (Wang et al. 2018, 2024), namely,

$$v_{Sk} = V_{\text{N3LO}}^{\text{C}} + V_{\text{N1LO}}^{\text{DD}}. \quad (5)$$

The central term is given by (Wang et al. 2018, 2024)

$$\begin{aligned} V_{\text{N3LO}}^{\text{C}} = & t_0 \left(1 + x_0 \hat{P}_\sigma \right) + t_1^{[2]} \left(1 + x_1^{[2]} \hat{P}_\sigma \right) \frac{1}{2} \left(\hat{k}'^2 + \hat{k}^2 \right) + t_2^{[2]} \left(1 + x_2^{[2]} \hat{P}_\sigma \right) \hat{k}' \cdot \hat{k} + t_1^{[4]} \left(1 + x_1^{[4]} \hat{P}_\sigma \right) \left[\frac{1}{4} \left(\hat{k}'^2 + \hat{k}^2 \right)^2 + \left(\hat{k}' \cdot \hat{k} \right)^2 \right] \\ & + t_2^{[4]} \left(1 + x_2^{[4]} \hat{P}_\sigma \right) \left(\hat{k}' \cdot \hat{k} \right) \left(\hat{k}'^2 + \hat{k}^2 \right) + t_1^{[6]} \left(1 + x_1^{[6]} \hat{P}_\sigma \right) \left(\hat{k}'^2 + \hat{k}^2 \right) \left[\frac{1}{2} \left(\hat{k}'^2 + \hat{k}^2 \right)^2 + 6 \left(\hat{k}' \cdot \hat{k} \right)^2 \right] \\ & + t_2^{[6]} \left(1 + x_2^{[6]} \hat{P}_\sigma \right) \left(\hat{k}' \cdot \hat{k} \right) \left[3 \left(\hat{k}'^2 + \hat{k}^2 \right)^2 + 4 \left(\hat{k}' \cdot \hat{k} \right)^2 \right], \end{aligned} \quad (6)$$

while the density-dependent term is expressed as (Wang et al. 2018, 2024)

$$V_{\text{N1LO}}^{\text{DD}} = \sum_{n=1,3,5} \frac{1}{6} t_3^{[n]} \left(1 + x_3^{[n]} \hat{P}_\sigma\right) \rho^{n/3}(\vec{R}), \quad (7)$$

where $\hat{P}_\sigma = (1 + \hat{\sigma}_1 \cdot \hat{\sigma}_2)/2$ is the spin-exchange operator; $\hat{k} = -i(\hat{\nabla}_1 - \hat{\nabla}_2)/2$ is the relative momentum operator; \hat{k}' is the conjugate operator of \hat{k} acting on the left; $\vec{R} = (\vec{r}_1 + \vec{r}_2)/2$; the $t_0, x_0, t_i^{[n]}, x_i^{[n]}$ ($n = 2, 4, 6$ and $i = 1, 2$), $t_3^{[n]}$ and $x_3^{[n]}$ ($n = 1, 3, 5$) are Skyrme parameters and thus there are totally twenty parameters. Note in Eqs. (6) and (7), the factor $\hat{\delta}(\vec{r}_1 - \vec{r}_1)$ is omitted for brevity.

In the mean-field approximation, the potential energy density for nucleon system with the extended N3LO Skyrme pseudopotential is given by (Wang et al. 2018, 2024)

$$\begin{aligned} V(\rho_n, \rho_p) = & \frac{1}{4} t_0 \left[(2 + x_0) \rho^2 - (2x_0 + 1) \sum_{\tau=n,p} \rho_\tau^2 \right] + \sum_{n=1,3,5} \frac{1}{24} t_3^{[n]} \left[(2 + x_3^{[n]}) \rho^2 - (2x_3^{[n]} + 1) \sum_{\tau=n,p} \rho_\tau^2 \right] \rho^{n/3} \\ & + \sum_{k=2,4,6} \left\{ \frac{C^{[k]}}{16\hbar^k(1 + \delta_{k4})} \int d^3p d^3p' (\vec{p} - \vec{p}')^k f(\vec{r}, \vec{p}) f(\vec{r}, \vec{p}') \right. \\ & + \frac{D^{[k]}}{16\hbar^k(1 + \delta_{k4})} \sum_{\tau=n,p} \int d^3p d^3p' (\vec{p} - \vec{p}')^k f_\tau(\vec{r}, \vec{p}) f_\tau(\vec{r}, \vec{p}') \\ & \left. + \sum_{m=0}^k (-1)^m \binom{k}{m} \left[\frac{E^{[k]}}{16(1 + \delta_{k4})} \nabla^m \rho \nabla^{k-m} \rho + \frac{F^{[k]}}{16(1 + \delta_{k4})} \sum_{\tau=n,p} \nabla^m \rho_\tau \nabla^{k-m} \rho_\tau \right] \right\}, \quad (8) \end{aligned}$$

where δ_{k4} denotes the Kronecker delta; $f_\tau(\vec{r}, \vec{p})$ is the nucleon phase distribution function; $C^{[n]}, D^{[n]}, E^{[n]}$ and $F^{[n]}$ are the combinations of Skyrme parameters $t_1^{[n]}, x_1^{[n]}, t_2^{[n]}, x_2^{[n]}$, i.e.

$$\begin{aligned} C^{[n]} &= t_1^{[n]} (2 + x_1^{[n]}) + t_2^{[n]} (2 + x_2^{[n]}), \\ D^{[n]} &= -t_1^{[n]} (2x_1^{[n]} + 1) + t_2^{[n]} (2x_2^{[n]} + 1), \\ E^{[n]} &= \frac{i^n}{2^n} \left[t_1^{[n]} (2 + x_1^{[n]}) - t_2^{[n]} (2 + x_2^{[n]}) \right], \\ F^{[n]} &= -\frac{i^n}{2^n} \left[t_1^{[n]} (2x_1^{[n]} + 1) + t_2^{[n]} (2x_2^{[n]} + 1) \right], \quad (9) \end{aligned}$$

with $n = 2, 4, 6$. Note that the number of parameters remains unchanged at twenty after the recombination. The single-nucleon potential can then be calculated as $U_\tau(\vec{r}, \vec{p}) = \delta V(\rho_n, \rho_p) / \delta \rho_\tau(\vec{r}, \vec{p})$ ($\tau = n$ or p).

In order to extend the newly developed N3LO Skyrme pseudopotential (Wang et al. 2018, 2024), which incorporates local, momentum-dependent, gradient and density-dependent terms, to the case of the octet baryons, it is convenient to rewrite the potential energy density in Eq. (8) in terms of explicit isospin index, in analogy to that of the momentum-dependent interaction (MDI) model (Das et al. 2003; Chen et al. 2005b; Xu et al. 2010b), namely,

$$\begin{aligned} V(\rho_n, \rho_p) = & A_u \rho_n \rho_p + \frac{A_l}{2} (\rho_n^2 + \rho_p^2) + \sum_{\alpha=1,3,5} \rho^{\alpha/3} \left[B_u^{[\alpha]} \rho_n \rho_p + \frac{B_l^{[\alpha]}}{2} (\rho_n^2 + \rho_p^2) \right] \\ & + \sum_{k=2,4,6} \left\{ \iint d^3p d^3p' (\vec{p} - \vec{p}')^k \left[\frac{M_u^{[k]}}{\hbar^k} f_n(\vec{r}, \vec{p}) f_p(\vec{r}, \vec{p}') + \frac{M_l^{[k]}}{2\hbar^k} (f_n(\vec{r}, \vec{p}) f_n(\vec{r}, \vec{p}') + f_p(\vec{r}, \vec{p}) f_p(\vec{r}, \vec{p}')) \right] \right. \\ & \left. + \sum_{m=0}^k (-1)^m \binom{k}{m} \left[G_u^{[k]} \nabla^m \rho_n \nabla^{k-m} \rho_p + \frac{G_l^{[k]}}{2} (\nabla^m \rho_n \nabla^{k-m} \rho_n + \nabla^m \rho_p \nabla^{k-m} \rho_p) \right] \right\}, \quad (10) \end{aligned}$$

where $A_u = \frac{t_0(2+x_0)}{2}$, $A_l = \frac{t_0(1-x_0)}{2}$, $B_u^{[\alpha]} = \frac{t_3^{[\alpha]}(2+x_3^{[\alpha]})}{12}$, $B_l^{[\alpha]} = \frac{t_3^{[\alpha]}(1-x_3^{[\alpha]})}{12}$, $M_u^{[k]} = \frac{C^{[k]}}{8(1+\delta_{k4})}$, $M_l^{[k]} = \frac{C^{[k]}+D^{[k]}}{8(1+\delta_{k4})}$, $G_u^{[k]} = \frac{E^{[k]}}{8(1+\delta_{k4})}$, $G_l^{[k]} = \frac{E^{[k]}+F^{[k]}}{8(1+\delta_{k4})}$, with $\alpha = (1, 3, 5)$ and $k = (2, 4, 6)$.

The explicit isospin index in Eq. (10) makes it easier to generalize the newly extended N3LO Skyrme pseudopotential to include the YN and YY interactions in terms of different baryon flavors. In particular, to incorporate hyperons into

the N3LO Skyrme pseudopotential, we assume that the YN and YY interactions have similar density, momentum, and isospin dependence as the NN interaction, and thus one can express the potential energy density contributions from any two types of octet baryons (b and b') utilizing the following form:

$$\begin{aligned}
V_{bb'} = & \sum_{\tau_b, \tau_{b'}} \left\{ \left(\frac{A_{bb'}}{2} \rho_{\tau_b} \rho_{\tau_{b'}} + \frac{A'_{bb'}}{2} \tau_b \tau_{b'} \rho_{\tau_b} \rho_{\tau_{b'}} \right) + \sum_{\alpha=1,3,5} \rho^{\frac{\alpha}{3}} \left(\frac{B_{bb'}^{[\alpha]}}{2} \rho_{\tau_b} \rho_{\tau_{b'}} + \frac{B'_{bb'}^{[\alpha]}}{2} \tau_b \tau_{b'} \rho_{\tau_b} \rho_{\tau_{b'}} \right) \right. \\
& + \sum_{k=2,4,6} \left[\iint d^3 p d^3 p' (\vec{p} - \vec{p}')^k \left(\frac{M_{bb'}^{[k]}}{2\hbar^k} f_{\tau_b}(\vec{r}, \vec{p}) f_{\tau_{b'}}(\vec{r}, \vec{p}') + \frac{M'_{bb'}^{[k]}}{2\hbar^k} \tau_b \tau_{b'} f_{\tau_b}(\vec{r}, \vec{p}) f_{\tau_{b'}}(\vec{r}, \vec{p}') \right) \right. \\
& \left. \left. + \sum_{m=0}^k (-1)^m \binom{k}{m} \left(\frac{G_{bb'}^{[k]}}{2} \nabla^m \rho_{\tau_b} \nabla^{k-m} \rho_{\tau_{b'}} + \frac{G'_{bb'}^{[k]}}{2} \tau_b \tau_{b'} \nabla^m \rho_{\tau_b} \nabla^{k-m} \rho_{\tau_{b'}} \right) \right] \right\}, \quad (11)
\end{aligned}$$

where b and b' represent the octet baryons (N, Λ, Σ, Ξ), and τ_b and $\tau_{b'}$ denote the third component of isospin for the corresponding octet baryons b and b' , respectively. Specifically, in this work, we assume $\tau_N = -1$ for neutrons and 1 for protons; $\tau_\Lambda = 0$ for Λ ; $\tau_\Sigma = -1, 0$ and 1 for Σ^-, Σ^0 and Σ^+ , respectively; $\tau_\Xi = -1$ for Ξ^- and 1 for Ξ^0 . For nucleonic system which only consists of neutrons and protons, the interaction parameters in Eq. (11) are given by

$$\begin{aligned}
A_{NN} &= \frac{A_l + A_u}{2}, \quad A'_{NN} = \frac{A_l - A_u}{2}, \\
X_{NN}^{[\alpha]} &= \frac{X_l^{[\alpha]} + X_u^{[\alpha]}}{2}, \quad X'_{NN}^{[\alpha]} = \frac{X_l^{[\alpha]} - X_u^{[\alpha]}}{2}, \quad (12)
\end{aligned}$$

where we have $X = B$ with $\alpha = (1, 3, 5)$, or $X = (M, G)$ with $\alpha = (2, 4, 6)$.

For octet baryons, we assume that the interaction parameters of YN and YY interactions are all proportional

to their corresponding counterparts in nucleon-nucleon interaction, namely

$$\begin{aligned}
A_{bb'} &= f_{A_{bb'}} A_{NN}, \quad A'_{bb'} = f_{A'_{bb'}} A'_{NN}, \\
X_{bb'}^{[\alpha]} &= f_{X_{bb'}^{[\alpha]}} X_{NN}^{[\alpha]}, \quad X'_{bb'}^{[\alpha]} = f_{X'_{bb'}^{[\alpha]}} X'_{NN}^{[\alpha]}, \quad (13)
\end{aligned}$$

and the meanings of X and α in Eq. (13) are the same as that in Eq. (12). The determination of the scaling parameters f , denoted by various subscripts in Eq. (13), will be discussed subsequently.

The total potential energy density of hypernuclear system can then be obtained by summing over all types of $V_{bb'}$ as

$$V_{HP} = \frac{1}{2} \sum_{b,b'} (1 + \delta_{bb'}) V_{bb'}. \quad (14)$$

By performing variation of V_{HP} , one can obtain the single-particle potential of the baryon species of τ_b , i.e.,

$$\begin{aligned}
U_{\tau_b}(p) &= \frac{\delta V_{HP}}{\delta \rho_{\tau_b}} \\
&= \sum_{b'} \sum_{\tau_{b'}} (1 + \delta_{bb'}) \left\{ \left(\frac{A_{bb'}}{2} \rho_{\tau_{b'}} + \frac{A'_{bb'}}{2} \tau_b \tau_{b'} \rho_{\tau_{b'}} \right) + \sum_{\alpha=1,3,5} \rho^{\frac{\alpha}{3}} \left(\frac{B_{bb'}^{[\alpha]}}{2} \rho_{\tau_{b'}} + \frac{B'_{bb'}^{[\alpha]}}{2} \tau_b \tau_{b'} \rho_{\tau_{b'}} \right) \right. \\
&+ \sum_{k=2,4,6} \left[\int d^3 p' (\vec{p} - \vec{p}')^k \left(\frac{M_{bb'}^{[k]}}{2\hbar^k} f_{\tau_{b'}}(\vec{r}, \vec{p}') + \frac{M'_{bb'}^{[k]}}{2\hbar^k} \tau_b \tau_{b'} f_{\tau_{b'}}(\vec{r}, \vec{p}') \right) \right. \\
&+ \left. \left(\frac{G_{bb'}^{[k]}}{2} 2^k \nabla^k \rho_{\tau_{b'}} \right) + \left. \left(\frac{G'_{bb'}^{[k]}}{2} 2^k \tau_b \tau_{b'} \nabla^k \rho_{\tau_{b'}} \right) \right] \right\} \\
&+ \frac{1}{2} \sum_{b'', b'''} \sum_{\tau_{b''}, \tau_{b'''}} (1 + \delta_{b'b''}) \left[\sum_{\alpha=1,3,5} \frac{\alpha}{3} \rho^{\frac{\alpha}{3}-1} \left(\frac{B_{b'b''}^{[\alpha]}}{2} \rho_{\tau_{b''}} \rho_{\tau_{b'''}} + \frac{B'_{b'b''}^{[\alpha]}}{2} \tau_b \tau_{b''} \rho_{\tau_{b''}} \rho_{\tau_{b'''}} \right) \right]. \quad (15)
\end{aligned}$$

2.3. Determination of parameters

In the present work, we mainly focus on infinite uniform nuclear and hypernuclear matter for which the gra-

dient terms vanish. For nuclear matter, by excluding the parameters associated with gradient terms (i.e., $E^{[2]}$, $E^{[4]}$, $E^{[6]}$, $F^{[2]}$, $F^{[4]}$, $F^{[6]}$, or equivalently $G_u^{[2]}$, $G_u^{[4]}$, $G_u^{[6]}$, $G_l^{[2]}$, $G_l^{[4]}$, $G_l^{[6]}$), the recently developed extended N3LO Skyrme pseudopotential for nucleons (Wang et al. 2024) can then be characterized solely by fourteen microscopic Skyrme parameters (or their combinations): t_0 , $t_3^{[1]}$, $t_3^{[3]}$, $t_3^{[5]}$, x_0 , $x_3^{[1]}$, $x_3^{[3]}$, $x_3^{[5]}$, $C^{[2]}$, $C^{[4]}$, $C^{[6]}$, $D^{[2]}$, $D^{[4]}$ and $D^{[6]}$, or equivalently A_u , A_l , $B_u^{[1]}$, $B_u^{[3]}$, $B_u^{[5]}$, $B_l^{[1]}$, $B_l^{[3]}$, $B_l^{[5]}$, $M_u^{[2]}$, $M_u^{[4]}$, $M_u^{[6]}$, $M_l^{[2]}$, $M_l^{[4]}$, $M_l^{[6]}$. These microscopic parameters can be determined by fourteen macroscopic quantities (Wang et al. 2024): ρ_0 , $E_0(\rho_0)$, K_0 , J_0 , a_2 , a_4 , a_6 , b_2 , b_4 , b_6 , $E_{\text{sym}}(\rho_0)$, L , K_{sym} and J_{sym} . Here, a_2 , a_4 and a_6 represent the polynomial momentum expansion coefficients of the single-nucleon potential (optical potential) in SNM at ρ_0 , namely $U_0(\rho_0, p)$, while b_2 , b_4 and b_6 correspond to those of the (first-order) nuclear symmetry potential at ρ_0 , namely $U_{\text{sym}}(\rho_0, p)$ (Wang et al. 2024):

$$U_0(\rho_0, p) = U_0(\rho_0, 0) + a_2 \left(\frac{p}{\hbar}\right)^2 + a_4 \left(\frac{p}{\hbar}\right)^4 + a_6 \left(\frac{p}{\hbar}\right)^6, \quad (16)$$

$$U_{\text{sym}}(\rho_0, p) = U_{\text{sym}}(\rho_0, 0) + b_2 \left(\frac{p}{\hbar}\right)^2 + b_4 \left(\frac{p}{\hbar}\right)^4 + b_6 \left(\frac{p}{\hbar}\right)^6. \quad (17)$$

In the above expressions, $U_0(\rho_0, 0)$, a_2 , a_4 and a_6 are determined by fitting the nucleon optical potential U_{opt} obtained from high energy nucleon-nucleus elastic scattering data, while $U_{\text{sym}}(\rho_0, 0)$, b_2 , b_4 and b_6 are obtained from fitting microscopic calculations, as detailed in Refs. (Wang et al. 2018, 2024). Following our previous work (Wang et al. 2024), we fix the values of those parameters, i.e., $a_2 = 6.52 \text{ MeV fm}^2$, $a_4 = -0.126 \text{ MeV fm}^4$, $a_6 = 8.13 \times 10^{-4} \text{ MeV fm}^6$, $b_2 = -3.00 \text{ MeV fm}^2$, $b_4 = 0.0780 \text{ MeV fm}^4$ and $b_6 = -7.00 \times 10^{-4} \text{ MeV fm}^6$. Note that both $U_0(\rho_0, 0)$ and $U_{\text{sym}}(\rho_0, 0)$ are not independent variables and their values are determined by the input macroscopic quantities via the Hugenholtz-Van Hove (HVH) theorem (Hugenholtz & van Hove 1958; Satpathy et al. 1999; Xu et al. 2010a; Chen et al. 2012; Cai & Chen 2012).

For the NN interaction parameters, apart from the six fixed polynomial momentum expansion coefficients of $U_0(\rho_0, p)$ and $U_{\text{sym}}(\rho_0, p)$ mentioned above, namely, a_2 , a_4 , a_6 , b_2 , b_4 , b_6 , we have also chosen $\rho_0 = 0.16 \text{ fm}^{-3}$, $E_0(\rho_0) = -16 \text{ MeV}$, $K_0 = 230 \text{ MeV}$, $J_0 = -383 \text{ MeV}$, $E_{\text{sym}}(\rho_0) = 32 \text{ MeV}$ and $L = 35 \text{ MeV}$ as default values. The default values of ρ_0 , $E_0(\rho_0)$, K_0 and J_0 for SNM are the same as those used in our previous work (Wang et al.

2024). Furthermore, setting $K_{\text{sym}} = -300 \text{ MeV}$ and $J_{\text{sym}} = 720 \text{ MeV}$, together with the default set of twelve macroscopic quantities: a_2 , a_4 , a_6 , b_2 , b_4 , b_6 , ρ_0 , $E_0(\rho_0)$, K_0 , J_0 , $E_{\text{sym}}(\rho_0)$ and L , leads to a standard interaction for nucleonic matter description, denoted as HSL35 in the present work. As we will see in the following, the interaction HSL35 not only satisfies the constraints of the mass-radius relation (for both NSs and HSs) from astrophysical observations but also aligns with the microscopic calculations regarding EOS of PNM. Further details will be discussed in the next section.

Once the interaction parameters of NN interaction are provided, one can determine the scaling parameters f by fitting the single-particle potential $U_b^{(b')}$, which represents the potential felt by a baryon b in the matter of baryon b' , to match the corresponding results obtained from experiments or microscopic calculations. The scaling parameters can be classified into various types according to whether they correspond to the local terms, the density-dependent terms or the momentum-dependent terms in the single-particle potential. In addition, these types of parameters can further be categorized according to whether the corresponding terms are isospin-dependent or isospin-independent. Although each parameter of the YN interaction has a unique corresponding scaling parameter f that may in principle be different from others, in the present work, we usually assume that the scaling parameters f are equal if they belong to the same class for the sake of simplicity. For instance, $f_{B_{N\Sigma}^{[1]}}$, $f_{B_{N\Sigma}^{[3]}}$ and $f_{B_{N\Sigma}^{[5]}}$ are all density-dependent but isospin-independent scaling parameters, and for simplicity, we assume that they are equal to each other and they are treated as a single free parameter.

For the ΛN interaction, there have relatively more reliable constraints on the potential of Λ in SNM (Kochankovski et al. 2024) compared to other hyperons. The isospin-dependent scaling parameters of Λ with primes in their superscripts are meaningless, as they are always multiplied by $\tau_\Lambda = 0$. The scaling parameter $f_{A_{N\Lambda}} = 1.36$ is obtained from fitting the Λ potential in SNM at saturation density and zero momentum (Millener et al. 1988; Friedman & Gal 2024):

$$U_\Lambda^{(N)}(\rho_N = \rho_0, p = 0) = -28 \text{ MeV}, \quad (18)$$

Furthermore, we obtain the scaling parameters $f_{B_{N\Lambda}^{[1]}} = f_{B_{N\Lambda}^{[3]}} = f_{B_{N\Lambda}^{[5]}} = 1.5$ by fitting the density dependence of the Λ potential in SNM [i.e., $U_\Lambda^{(N)}(\rho_N, p = 0)$] around ρ_0 predicted by χEFT (Petschauer et al. 2016). Similarly, to reproduce the momentum dependence of the Λ potential in SNM at ρ_0 [i.e., $U_\Lambda^{(N)}(\rho_N = \rho_0, p)$] given by χEFT , we fix $f_{M_{N\Lambda}^{[2]}} = f_{M_{N\Lambda}^{[4]}} = f_{M_{N\Lambda}^{[6]}} = 1.60$.

For the ΣN interaction, to reproduce the density dependence of Σ potential (at zero momentum) around ρ_0 in SNM predicted by χ EFT (Petschauer et al. 2016), we fix $f_{B_{N\Sigma}^{[1]}} = f_{B_{N\Sigma}^{[3]}} = f_{B_{N\Sigma}^{[5]}} = 1.30$. Then we choose (Petschauer et al. 2016)

$$U_{\Sigma}^{(N)}(\rho_N = \rho_0, p = 0) = 11 \text{ MeV} \quad (19)$$

in SNM and

$$U_{\Sigma^-}^{(N)}(\rho_N = \rho_0, p = 0) = 40 \text{ MeV} \quad (20)$$

in PNM, which leads to $f_{A_{N\Sigma}} = 0.88$ and $f_{A'_{N\Sigma}} = f_{B_{N\Sigma}^{[1]}} = f_{B_{N\Sigma}^{[3]}} = f_{B_{N\Sigma}^{[5]}} = 2.41$, respectively. Additionally, we set $f_{M_{N\Sigma}^{[2]}} = f_{M_{N\Sigma}^{[4]}} = f_{M_{N\Sigma}^{[6]}} = 1.10$ and $f_{M_{N\Sigma}^{[2]'}} = f_{M_{N\Sigma}^{[4]'}} = f_{M_{N\Sigma}^{[6]'}} = 3.70$, based on the momentum dependence of Σ at ρ_0 in SNM and of Σ^- at ρ_0 in PNM, calculated using χ EFT.

The procedure for determining the scaling parameters of the ΞN interaction is analogous to that for the ΣN interaction. It should be noted that while there exist calculations of the potentials for the ΞN interaction using LQCD (Inoue 2019), no such calculations have been performed using χ EFT. Consequently, we select the following LQCD results for the ΞN interaction (Inoue 2019), i.e.,

$$U_{\Xi}^{(N)}(\rho_N = \rho_0, p = 0) = -4 \text{ MeV} \quad (21)$$

in SNM and

$$U_{\Xi^-}^{(N)}(\rho_N = \rho_0, p = 0) = 7 \text{ MeV} \quad (22)$$

in PNM, which respectively lead to $f_{A_{N\Xi}} = f_{B_{N\Xi}^{[1]}} = f_{B_{N\Xi}^{[3]}} = f_{B_{N\Xi}^{[5]}} = 0.52$ and $f_{A'_{N\Xi}} = f_{B_{N\Xi}^{[1]}} = f_{B_{N\Xi}^{[3]}} = f_{B_{N\Xi}^{[5]}} = 1.25$. By setting $f_{M_{N\Xi}^{[2]}} = f_{M_{N\Xi}^{[4]}} = f_{M_{N\Xi}^{[6]}} = 0.20$, we can reproduce the momentum dependence of Ξ in SNM at ρ_0 , as predicted by LQCD. Similarly, when fixing $f_{M_{N\Xi}^{[2]'}} = f_{M_{N\Xi}^{[4]'}} = f_{M_{N\Xi}^{[6]'}} = 0.50$, a relatively good fit is achieved for the momentum dependence of Ξ^- in PNM at ρ_0 , as obtained from LQCD.

The empirical ranges of $U_Y^{(N)}(\rho_N = \rho_0, p = 0)$ for Σ and Ξ in SNM are estimated to approximately be (10, 50) MeV and (-24, -10) MeV (Friedman & Gal 2007, 2021; Kochankovski et al. 2024), respectively. Although the chosen value of Ξ from LQCD falls slightly outside its empirical range, our aforementioned choices remain acceptable due to the large uncertainties regarding Ξ properties. Nevertheless, we have checked that varying $U_{\Xi}^{(N)}(\rho_N = \rho_0, p = 0)$ from -4 to -16 MeV (by factor four) only has small effects and does not change our conclusion.

Finally, there exists six types of YY interactions, which are poorly known for the moment. To simplify

the problem for a given YY interaction, we assume that the scaling parameters belonging to different classes are identical and only one adjustable scaling parameter exists. The single scaling parameter can be determined using the equation concerning $U_Y^{(Y')}(\rho_{Y'} = \rho_0, p = 0)$ in symmetric hypernuclear matter, similar to the approach employed for YN interaction. Since the properties of the YY interaction are still ambiguous at present, following Refs. (Schaffner et al. 1994; Xu et al. 2010b), we simply set

$$U_Y^{(Y')}(\rho_{Y'} = \rho_0, p = 0) = -40 \text{ MeV}. \quad (23)$$

We note that varying the above value by factor two only has minor effects on our results.

In Fig. 1, we present the single-particle potentials of various octet baryons obtained using the HSL35 interaction, alongside the experimentally derived nucleon optical potential (Hama et al. 1990; Cooper et al. 1993), the calculations based on chiral effective field theory (Petschauer et al. 2016) and the results from LQCD (Inoue 2019). It is seen from Fig. 1 that the interaction HSL35 can reasonably describe the density and momentum dependence of the single-particle potentials for various octet baryons. It should be pointed out that when we fix $U_{\Sigma}^{(N)}(\rho_N = \rho_0)$ in SNM as shown in Eq. (19) and $U_{\Sigma^-}^{(N)}(\rho_N = \rho_0)$ in PNM as shown in Eq. (20), $U_{\Sigma^0}^{(N)}(\rho_N = \rho_0)$ and $U_{\Sigma^+}^{(N)}(\rho_N = \rho_0)$ have then also been fixed accordingly within the energy density functional used in our present work. Similarly, $U_{\Xi^0}^{(N)}(\rho_N = \rho_0)$ is then determined accordingly once $U_{\Xi}^{(N)}(\rho_N = \rho_0)$ and $U_{\Xi^-}^{(N)}(\rho_N = \rho_0)$ are fixed as shown in Eq. (21) and Eq. (22), respectively. As a result, the momentum dependence of Σ^- in PNM can be reproduced relatively more accurately than that of Σ^0 and Σ^+ , and the momentum dependence of Ξ^- is reproduced better than that of Ξ^0 , as the potentials of Σ^- and Ξ^- in PNM have been used in our parameter calibration. Nevertheless, because of the uncertainty associated with hyperonic interactions, the HSL35 interaction already provides a reasonable description of both experimental data and microscopic calculations overall.

In Table 1, we list the parameters for the NN interaction in Eq. (11), as well as the scaling parameters f for the YN and YY interactions. These parameters are all derived from the standard interaction HSL35. It is worth noting that while varying K_{sym} and J_{sym} may impact the parameters of the NN interaction, it does not change the scaling parameters f whose values are assumed to be fixed at the corresponding ones in the HSL35 interaction.

2.4. Beta-stable hypernuclear matter

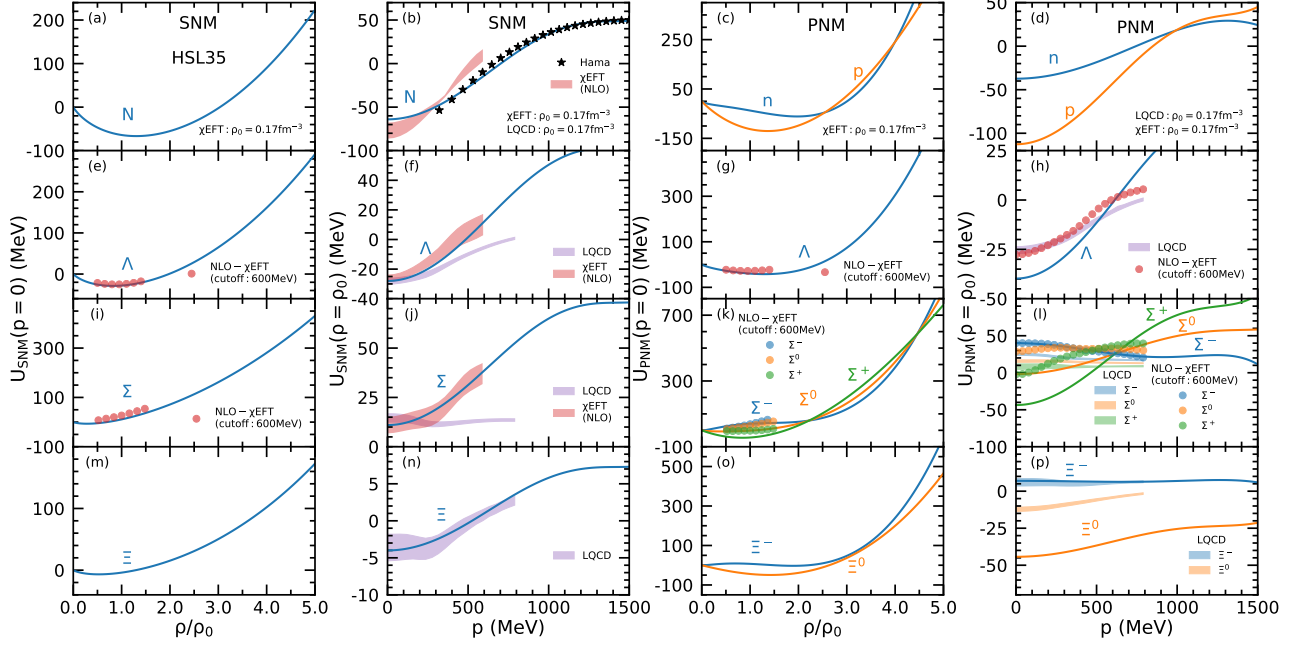


Figure 1. The density (first and third columns) and momentum (second and fourth columns) dependence of single-particle potentials for octet baryons in SNM (left two columns) and PNM (right two columns) with the HSL35 interaction. The experimental nucleon optical potential (Hama et al. 1990; Cooper et al. 1993), the calculations from χ EFT (Petschauer et al. 2016) and LQCD (Inoue 2019) are also included for comparison.

Table 1. Parameters for the NN interaction and the scaling parameters f for the NN, YN and YY interactions in the HSL35 interaction. Here, $f_{X_{NN}}$ and $f_{X_{YY}}$ represent the scaling parameters for the NN and YY interaction, respectively, and they are universal and independent of the different terms for NN and YY interactions. The units of the parameters for NN interaction are as follows: A_{NN} and A'_{NN} : MeV fm³; $B_{NN}^{[n]}$ and $B'_{NN}^{[n]}$: MeV fmⁿ⁺³ ($n = 1, 3, 5$); $M_{NN}^{[n]}$ and $M'_{NN}^{[n]}$: MeV fmⁿ⁺³ ($n = 2, 4, 6$). It is important to note that all scaling parameters denoted by f are dimensionless.

A_{NN}	$B_{NN}^{[1]}$	$B_{NN}^{[3]}$	$B_{NN}^{[5]}$	A'_{NN}	$B'_{NN}^{[1]}$	$B'_{NN}^{[3]}$	$B'_{NN}^{[5]}$	$M_{NN}^{[2]}$	$M_{NN}^{[6]}$	$M_{NN}^{[4]}$	$M'_{NN}^{[2]}$	$M'_{NN}^{[4]}$	$M'_{NN}^{[6]}$
-1380.34	1626.28	-504.55	298.29	52.13	1439.44	-4591.59	3637.27	43.62	-0.83	0.0051	-21.86	0.54	-0.0044
$f_{A_{N\Lambda}}$	$f_{B_{N\Lambda}^{[1]}}, f_{B_{N\Lambda}^{[3]}}, f_{B_{N\Lambda}^{[5]}}$			$f_{A'_{N\Lambda}}, f_{B'_{N\Lambda}^{[1]}}, f_{B'_{N\Lambda}^{[3]}}, f_{B'_{N\Lambda}^{[5]}}$				$f_{M_{N\Lambda}^{[2]}}, f_{M_{N\Lambda}^{[4]}}, f_{M_{N\Lambda}^{[6]}}$			$f_{M'_{N\Lambda}^{[2]}}, f_{M'_{N\Lambda}^{[4]}}, f_{M'_{N\Lambda}^{[6]}}$		
1.36	1.50			—				1.60			—		
$f_{A_{N\Sigma}}$	$f_{B_{N\Sigma}^{[1]}}, f_{B_{N\Sigma}^{[3]}}, f_{B_{N\Sigma}^{[5]}}$			$f_{A'_{N\Sigma}}, f_{B'_{N\Sigma}^{[1]}}, f_{B'_{N\Sigma}^{[3]}}, f_{B'_{N\Sigma}^{[5]}}$				$f_{M_{N\Sigma}^{[2]}}, f_{M_{N\Sigma}^{[4]}}, f_{M_{N\Sigma}^{[6]}}$			$f_{M'_{N\Sigma}^{[2]}}, f_{M'_{N\Sigma}^{[4]}}, f_{M'_{N\Sigma}^{[6]}}$		
0.88	1.30			2.41				1.10			3.70		
$f_{A_{N\Xi}}, f_{B_{N\Xi}^{[1]}}, f_{B_{N\Xi}^{[3]}}, f_{B_{N\Xi}^{[5]}}$				$f_{A'_{N\Xi}}, f_{B'_{N\Xi}^{[1]}}, f_{B'_{N\Xi}^{[3]}}, f_{B'_{N\Xi}^{[5]}}$				$f_{M_{N\Xi}^{[2]}}, f_{M_{N\Xi}^{[4]}}, f_{M_{N\Xi}^{[6]}}$			$f_{M'_{N\Xi}^{[2]}}, f_{M'_{N\Xi}^{[4]}}, f_{M'_{N\Xi}^{[6]}}$		
0.52				1.25				0.20			0.50		
$f_{X_{NN}}$		$f_{X_{\Lambda\Lambda}}$		$f_{X_{\Sigma\Sigma}}$		$f_{X_{\Xi\Xi}}$		$f_{X_{\Sigma\Lambda}}$		$f_{X_{\Xi\Lambda}}$		$f_{X_{\Xi\Sigma}}$	
1.00		0.67		0.61		0.62		1.33		1.33		1.22	

The stable hyperon star matter satisfies the conditions of baryon number conservation, charge neutrality, and β -equilibrium:

$$\begin{aligned}
 \sum_i \rho_i b_i &= \rho_B, \\
 \sum_i \rho_i q_i &= 0, \\
 \mu_i &= \mu_b b_i - \mu_q q_i.
 \end{aligned}
 \tag{24}$$

In the above expressions, the subscript i denotes the particle species, including nucleons, hyperons and leptons. In this study, we assume that the hyperon star matter is neutrino free and the lepton category comprises electrons and muons. The b_i , q_i and μ_i represent the baryon number, (electric) charge number and chemical potential of the corresponding particles. Due to the above equilibrium conditions, only two independent chemical potentials exist, i.e., the baryon chemical potential μ_b

and the charge chemical potential μ_q . In addition, the ρ_B corresponds to the total baryon number density.

For interacting octet baryon matter at zero temperature, the chemical potential of species τ_b can be expressed as follows:

$$\mu_{\tau_b}(p_{F\tau_b}) = m_{\tau_b} + \frac{p_{F\tau_b}^2}{2m_{\tau_b}} + U_{\tau_b}(p_{F\tau_b}), \quad (25)$$

where m_{τ_b} and $p_{F\tau_b}$ represent the baryon's rest mass and Fermi momentum, respectively. The leptons are considered as relativistic free Fermi gas, and their chemical potentials are given by

$$\mu_l(p_{Fl}) = \sqrt{m_l^2 + p_{Fl}^2}. \quad (26)$$

The Fermi momentum of species i can be determined using the formula $p_{Fi} = (3\pi^2\rho_i)^{1/3}$. By substituting the chemical potential formulae into Eq. (24) and solving for different total baryon densities ρ_B , one can then obtain the particle fractions of species i , denoted as ρ_i/ρ_B . The total energy density ϵ consists of two components:

$$\epsilon = \epsilon_H + \epsilon_L, \quad (27)$$

where ϵ_H and ϵ_L denote the energy density of baryons and leptons, respectively. Except for the total potential energy density of baryons V_{HP} given in Eq. (14), the mass term ϵ_{HM} and kinetic energy term ϵ_{HK} also contribute to ϵ_H , which are computed by

$$\begin{aligned} \epsilon_H &= \epsilon_{HM} + \epsilon_{HK} + V_{HP}, \\ \epsilon_{HK} &= \sum_b \sum_{\tau_b} \frac{2}{(2\pi)^3} \int_0^{p_{F\tau_b}} \left(\frac{p^2}{2m_{\tau_b}}\right) (4\pi p^2) dp \\ &= \sum_b \sum_{\tau_b} \frac{p_{F\tau_b}^5}{10\pi^2 m_{\tau_b}}, \\ \epsilon_{HM} &= \sum_b \sum_{\tau_b} \rho_{\tau_b} m_{\tau_b}. \end{aligned} \quad (28)$$

Since the electron's mass is very small, we treat the electron as massless particle, and the energy for a free electron can be approximated as $\sqrt{m_e^2 + p_e^2} \approx p_e$. Consequently, the energy density of leptons can be expressed as:

$$\begin{aligned} \epsilon_L &= \epsilon_e + \epsilon_\mu, \\ \epsilon_e &= \frac{2}{(2\pi)^3} \int_0^{p_{Fe}} (p) (4\pi p^2) dp = \frac{p_{Fe}^4}{4\pi^2}, \\ \epsilon_\mu &= \frac{2}{(2\pi)^3} \int_0^{p_{F\mu}} (\sqrt{m_\mu^2 + p^2}) (4\pi p^2) dp \\ &= \frac{1}{4\pi^2} \left[p_{F\mu} \mu_\mu^3 - \frac{1}{2} m_\mu^2 p_{F\mu} \mu_\mu \right. \\ &\quad \left. - \frac{1}{2} m_\mu^4 \ln \left(\frac{p_{F\mu} + \mu_\mu}{m_\mu} \right) \right]. \end{aligned} \quad (29)$$

According to the fundamental thermodynamic relation, the total pressure of β -stable and charge-neutral hypernuclear matter can be derived as follows:

$$P = \left(\sum_b \sum_{\tau_b} \mu_{\tau_b} \rho_{\tau_b} + \sum_l \mu_l \rho_l \right) - (\epsilon_H + \epsilon_L). \quad (30)$$

The thermodynamic consistency condition $P = \rho_B^2 \frac{d(\epsilon/\rho_B)}{d\rho_B}$ can also be verified using the aforementioned formulae.

To calculate the properties of NSs and HSs, one also needs the explicit information on the crust EOS. In the present work, the core-crust transition density ρ_t , which separates the liquid core from the nonuniform inner crust, is determined self-consistently via the so-called dynamical method of Ref. (Xu et al. 2009a). In addition, the critical density between the inner and outer crusts is taken to be $\rho_{\text{out}} = 2.46 \times 10^{-4} \text{ fm}^{-3}$ (Carriere et al. 2003; Xu et al. 2009a,b). For the outer crust with $\rho < \rho_{\text{out}}$, we adopt the famous BPS (FMT) EOS (Baym et al. 1971; Iida & Sato 1997); for the inner crust with $\rho_{\text{out}} < \rho < \rho_t$, where the so-called nuclear pasta could appear, we assume a parameterized EOS with the polytropic form $P = a + b\epsilon^{4/3}$ with a and b determined from the EOS at ρ_{out} and ρ_t (Carriere et al. 2003; Xu et al. 2009a,b).

3. RESULTS AND DISCUSSIONS

As discussed previously, for infinite uniform nucleonic matter system, the N3LO Skyrme pseudopotential EDF has totally fourteen parameters, i.e., $t_0, t_3^{[1]}, t_3^{[3]}, t_3^{[5]}, x_0, x_3^{[1]}, x_3^{[3]}, x_3^{[5]}, C^{[2]}, C^{[4]}, C^{[6]}, D^{[2]}, D^{[4]}$ and $D^{[6]}$ (or equivalently $A_u, A_l, B_u^{[1]}, B_u^{[3]}, B_u^{[5]}, B_l^{[1]}, B_l^{[3]}, B_l^{[5]}, M_u^{[2]}, M_u^{[4]}, M_u^{[6]}, M_l^{[2]}, M_l^{[4]}, M_l^{[6]}$), which can be uniquely determined by fourteen macroscopic quantities (Wang et al. 2024): $\rho_0, E_0(\rho_0), K_0, J_0, a_2, a_4, a_6, b_2, b_4, b_6, E_{\text{sym}}(\rho_0), L, K_{\text{sym}}$ and J_{sym} . In this work, our main motivation is to investigate how the high density symmetry energy influences the properties of HSs. To this end, we primarily explore the impact of the higher order symmetry energy parameters K_{sym} and J_{sym} , which are used to feature the high density behavior of the symmetry energy, while keep the remaining twelve macroscopic quantities [i.e., $\rho_0, E_0(\rho_0), K_0, J_0, a_2, a_4, a_6, b_2, b_4, b_6, E_{\text{sym}}(\rho_0)$ and L] fixed at their respective values in the standard interaction HSL35.

Before presenting the detailed results on NSs and HSs, we would like to mention some features about the EOS of SNM as well as the values of $E_{\text{sym}}(\rho_0)$ and L for the standard interaction HSL35. Firstly, for the properties of SNM, the HSL35 prediction on pressure as a function of density up to about $5\rho_0$ is strictly in agreement with

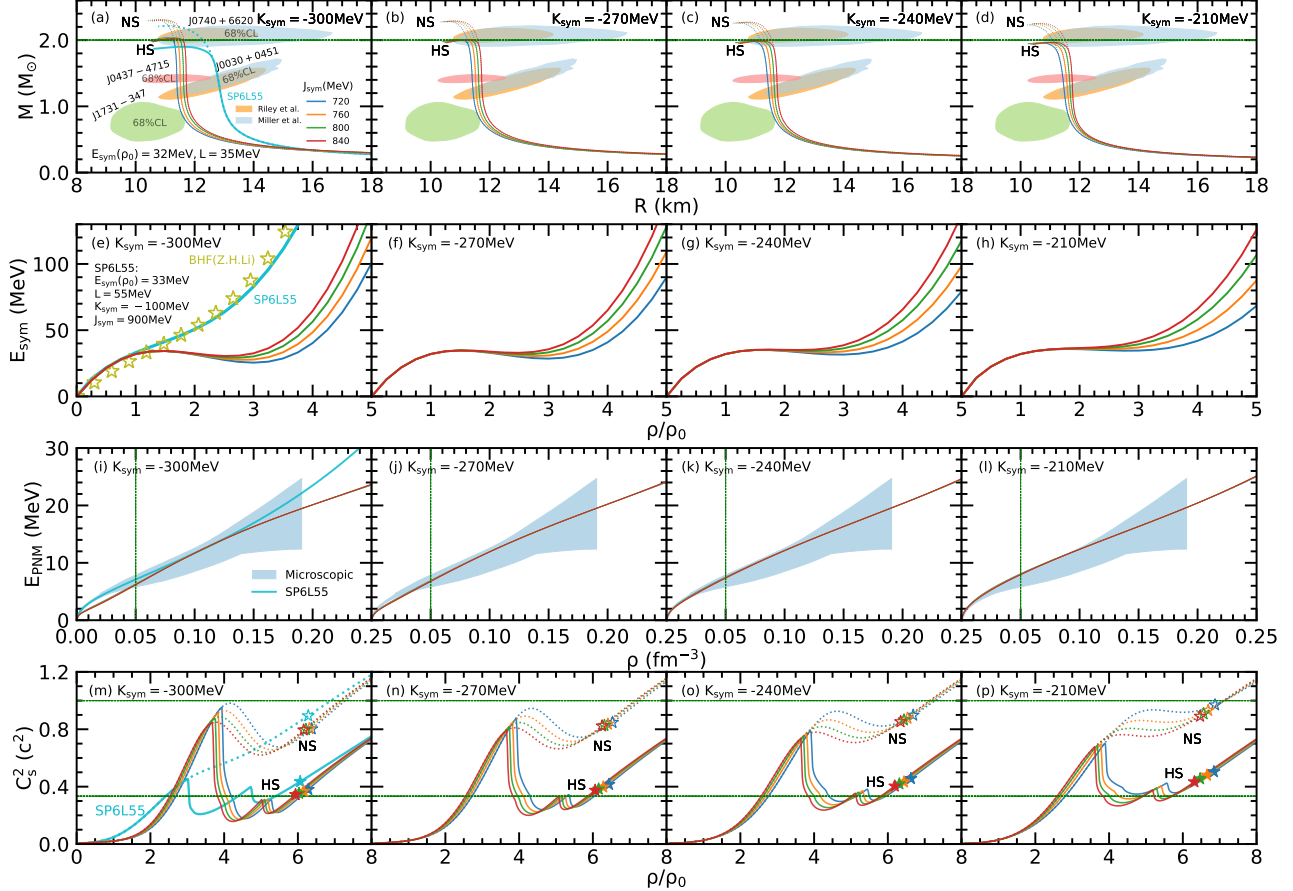


Figure 2. The mass-radius relation for static HSs and NSs (first row), density dependence of the symmetry energy $E_{\text{sym}}(\rho)$ (second row), the EOS of PNM $E_{\text{PNM}}(\rho)$ (third row) and density dependence of the sound speed squared $C_s^2(\rho/\rho_0)$ (fourth row) by varying individually K_{sym} and J_{sym} in the HSL35 interaction. The corresponding results with SP6L55 are included in the first column. The symmetry energy from the microscopic BHF calculation, denoted by BHF(Z.H.Li), is shown in panel (e). The stars in the lowest row indicate the corresponding densities at the center of NSs and HSs with maximum mass configuration. For comparison, some typical constraints from astrophysical observations and microscopic calculations are included in the first and third rows, respectively. Further details can be found in the text.

the constraints extracted from flow data in high-energy HICs (Danielewicz et al. 2002), as depicted in Fig. 1 of our previous work (Wang et al. 2024). Secondly, for the magnitude of the symmetry energy at nuclear saturation density, we take its value to be $E_{\text{sym}}(\rho_0) = 32$ MeV for HSL35, since this is a widely accepted value for $E_{\text{sym}}(\rho_0)$. Thirdly, for the slope parameter L , it is shown (Wang et al. 2024) that a value of L significantly larger than 35 MeV will lead to an inconsistency with the mass-radius relation from the observation of HESS J1731-347 (Doroshenko et al. 2022). Conversely, if L falls far below 35 MeV, it becomes impossible to simultaneously satisfy both constraints imposed on the mass-radius relation for PSR J0030+0451 (Miller et al. 2019; Riley et al. 2019) and PSR J0740+6620 (Miller et al. 2021; Riley et al. 2021) along with EOS of PNM derived through microscopic calculations (Huth et al. 2021; Zhang & Chen 2023).

By varying individually K_{sym} and J_{sym} in HSL35 with K_{sym} spanning from -300 to -210 MeV in an interval of 30 MeV whereas J_{sym} spanning from 720 to 840 MeV in an interval of 40 MeV, we show in Fig. 2 the mass-radius relation for HSs and NSs [in panels (a), (b), (c) and (d)], the density dependence of the symmetry energy [in panels (e), (f), (g) and (h)], the EOS of PNM [in panels (i), (j), (k) and (l)] and the speed of sound squared as a function of density for HS and NS matter [in panels (m), (n), (o) and (p)]. Also included in panels (a) - (d) of Fig. 2 are the constraints of the mass-radius relation obtained from astrophysical observations on PSR J0030+0451 ($M \approx 1.4M_\odot$) (Miller et al. 2019; Riley et al. 2019), PSR J0740+6620 ($M \approx 2M_\odot$) (Miller et al. 2021; Riley et al. 2021) and the recently reported PSR J0437-4715 ($M \approx 1.4M_\odot$) (Choudhury et al. 2024) by NICER, as well as on the central compact object with a mass around $0.77M_\odot$ in the supernova remnant HESS

J1731-347 (Doroshenko et al. 2022), at a confidence level (C.L.) of 68%. In addition, we also present, in Fig. 2 (i) - (l), the combined constraint on $E_{\text{PNM}}(\rho)$ incorporating various microscopic calculations (Huth et al. 2021; Zhang & Chen 2023).

The case with $K_{\text{sym}} = -300$ MeV and $J_{\text{sym}} = 720$ MeV shown in the first column of Fig. 2 [i.e., panels (a), (e), (i) and (m)] corresponds to the HSL35 interaction. It is seen that the HSL35 interaction predicts $M_{\text{TOV}} = 2.04$ (2.31) M_{\odot} for HSs (NSs) and at the same time it can nicely describe the mass-radius relations obtained from astrophysical observations, especially the unusually low mass and small radius of HESS J1731-347. Furthermore, the HSL35 interaction is also compatible with the microscopic calculation constraint on the $E_{\text{PNM}}(\rho)$ at density region of $\rho \gtrsim 0.05$ fm $^{-3}$. Note that at lower densities (e.g., below about 0.05 fm $^{-3}$), the pairing effects, which are not considered in the mean-field calculations for $E_{\text{PNM}}(\rho)$, may become considerable (Zhang & Chen 2019). Moreover, one sees although the sound speed squared (C_s^2) of NS matter exceeds the vacuum light speed squared (c^2) at very high densities, the C_s^2 at densities below the central density of the NS with M_{TOV} remains smaller than c^2 , and so the causality condition is satisfied, guaranteeing that our results remain physically valid. Therefore, the HSL35 interaction provides a solution to the hyperon puzzle.

Now let's see how the higher order symmetry energy parameters K_{sym} and J_{sym} influence our results. From the first row of Fig. 2 [i.e., panels (a), (b), (c) and (d)], one can see that the M_{TOV} for both NSs and HSs decreases with the increment of the K_{sym} . In particular, the M_{TOV} of HSs (NSs) are 2.04 (2.31) M_{\odot} , 2.01 (2.28) M_{\odot} , 1.98 (2.26) M_{\odot} and 1.96 (2.23) M_{\odot} for $K_{\text{sym}} = -300, -270, -240$ and -210 MeV, respectively, for a fixed value of $J_{\text{sym}} = 720$ MeV. Therefore, the M_{TOV} of HSs becomes smaller than $2M_{\odot}$ when K_{sym} is larger than -240 MeV. In addition, we note a large K_{sym} (e.g., $K_{\text{sym}} > -210$ MeV) will violate the constraint on $E_{\text{PNM}}(\rho)$ from microscopic calculations (Huth et al. 2021; Zhang & Chen 2023). As to the effects of J_{sym} , while the J_{sym} has obvious effects on the radius of NSs and HSs with a larger J_{sym} leading to a larger radius, it only has minor effects on the M_{TOV} for both NSs and HSs. For example, the M_{TOV} of HSs (NSs) are 2.04 (2.31) M_{\odot} , 2.03 (2.31) M_{\odot} , 2.03 (2.31) M_{\odot} and 2.03 (2.31) M_{\odot} for $J_{\text{sym}} = 720, 760, 800$ and 840 MeV, respectively, for a fixed value of $K_{\text{sym}} = -300$ MeV. We note that the observed small radius of HESS J1731-347 cannot be obtained when J_{sym} is larger than about 760 MeV. On the other hand, a small J_{sym} will predict a too small radius for PSR J0030+0451 ($M \approx 1.4M_{\odot}$)

to conform to the measured value by NICER (Miller et al. 2019). These analyses and discussions suggest that a symmetry energy with $K_{\text{sym}} \approx -300$ MeV and $J_{\text{sym}} \approx 720$ MeV, together with $E_{\text{sym}}(\rho_0) \approx 32$ MeV and $L \approx 35$ MeV, can support massive HSs with $M_{\text{TOV}} \gtrsim 2M_{\odot}$ and simultaneously it is compatible with the astrophysical constraints on the mass-radius relations by NICER and HESS J1731-347 as well as the microscopic calculations on $E_{\text{PNM}}(\rho)$.

From the second row of Fig. 2 [i.e., panels (e), (f), (g) and (h)], it is seen that the symmetry energy with $K_{\text{sym}} \approx -300$ MeV and $J_{\text{sym}} \approx 720$ MeV (together with $E_{\text{sym}}(\rho_0) \approx 32$ MeV and $L \approx 35$ MeV) displays a quite soft density behavior around $2 - 3\rho_0$ but very stiff one above $4\rho_0$. The fast stiffening of the symmetry energy at high density is necessary to support a massive NS with mass larger than $2M_{\odot}$, given that the symmetry energy is soft at intermediate densities. It is interesting to see from the lowest row of Fig. 2 [i.e., panels (m), (n), (o) and (p)] that the softening of the symmetry energy around $2 - 3\rho_0$ with smaller values of K_{sym} and J_{sym} can push the critical density for hyperon appearance to a larger value and thus leads to a larger M_{TOV} for HSs. In addition, the hyperon appearance softens significantly the EOS of HS matter and thus leads to a clear peak for the sound speed squared around $4\rho_0$, which provides a natural explanation for the similar peak structure for sound speed squared observed in Bayesian model-agnostic analysis on the multi-messenger data of NSs together with ab initio calculations from perturbative quantum chromodynamics and chiral effective field theory [(see, e.g., Ref. (Cao & Chen 2023))].

Our results indicate that the softening of the symmetry energy at intermediate densities (around $2 - 3\rho_0$) plays an important role in enhancing the critical density for hyperon appearance and increasing the M_{TOV} of HSs. For comparison, we include the corresponding results in the first column of Fig. 2 [i.e., panels (a), (e), (i) and (m)] from a conventional interaction SP6L55 constructed in our previous work (Wang et al. 2024), for which the fourteen macroscopic quantities [i.e., $\rho_0, E_0(\rho_0), K_0, J_0, a_2, a_4, a_6, b_2, b_4, b_6, E_{\text{sym}}(\rho_0), L, K_{\text{sym}}$ and J_{sym}] are the same as those of the standard interaction HSL35 except for $E_{\text{sym}}(\rho_0) = 33$ MeV, $L = 55$ MeV, $K_{\text{sym}} = -100$ MeV and $J_{\text{sym}} = 900$ MeV, and so the SP6L55 has a much stiffer symmetry energy around intermediate densities compared to the HSL35 [see Fig. 2 (e)]. Also included in Fig. 2 (e) is the symmetry energy from the microscopic Brueckner-Hartree-Fock calculations using the Bonn B nucleon-nucleon potentials together with compatible microscopic meson-exchange three-body forces, denoted as BHF(Z.H.Li) (Li

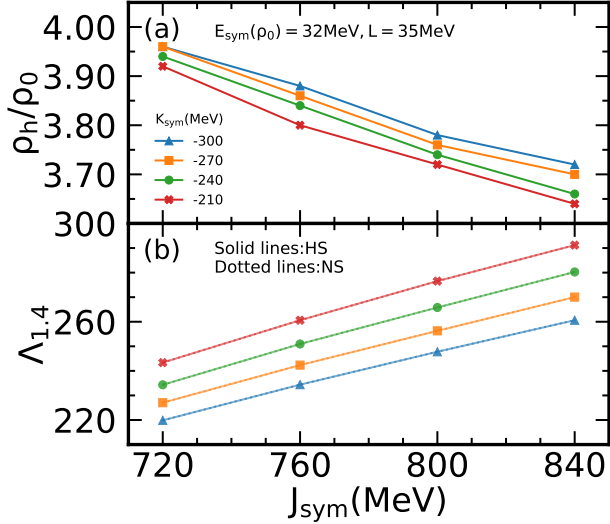


Figure 3. The critical density ρ_h for hyperon appearance in NS matter (a) and the tidal deformability $\Lambda_{1.4}$ of $1.4M_\odot$ NSs and HSs by varying individually K_{sym} and J_{sym} in the HSL35 interaction. Note the $\Lambda_{1.4}$ of NSs is the same as that of HSs and thus the symbols for NSs and HSs in panel (b) are exactly coincided. See the text for more details.

& Schulze 2008). One sees that the density behavior of the symmetry energy for SP6L55 is very similar to that of BHF(Z.H.Li). The SP6L55 predicts qualitatively different symmetry energy from the HSL35, and it gives a $M_{\text{TOV}} = 1.90(2.21)M_\odot$ for HSs (NSs) and a large radius of about 13 km at $M \approx 0.6 \sim 1.8M_\odot$, failing to conform to the observed maximum mass for pulsars and the astrophysical constraints on the mass-radius relation. Compared to HSL35, the SP6L55 predict a much smaller critical density, namely, $\sim 3\rho_0$ for hyperon appearance, as shown in Fig. 2 (m), which softens the EOS of HS matter and thus leads to a smaller M_{TOV} for HSs.

In order to see more clearly the effects of K_{sym} and J_{sym} on the properties of NSs and HSs, we show in Fig. 3 the critical density for hyperon appearance in HS matter and the tidal deformability for NSs and HSs with mass of $1.4M_\odot$ by varying individually K_{sym} and J_{sym} in the HSL35 interaction. It is seen from Fig. 3 (a) that a larger value of K_{sym} or J_{sym} leads systematically to a smaller hyperon emergence density, as we have observed and discussed above on the sound speed squared shown in the lowest row of Fig. 2. Furthermore, as depicted in Fig. 3 (b), it is evident that the dimensionless tidal deformability $\Lambda_{1.4}$ of a $1.4M_\odot$ star for both HSs and NSs is in nice agreement with the limit extracted from gravitational wave signal GW170817, namely 190^{+390}_{-120} (Abbott et al. 2018) as reported by LIGO and Virgo Collaboration. Note that in Fig. 3 (b), the tidal deformability $\Lambda_{1.4}$ of HSs is exactly the same as that of NSs, due to

the smaller central density in $1.4M_\odot$ HSs below which the hyperons have not yet appear in the HS matter. Our results therefore indicate that the tidal deformability for both HSs and NSs with HSL35 is nicely compatible with the constraint extracted from gravitational wave signal GW170817.

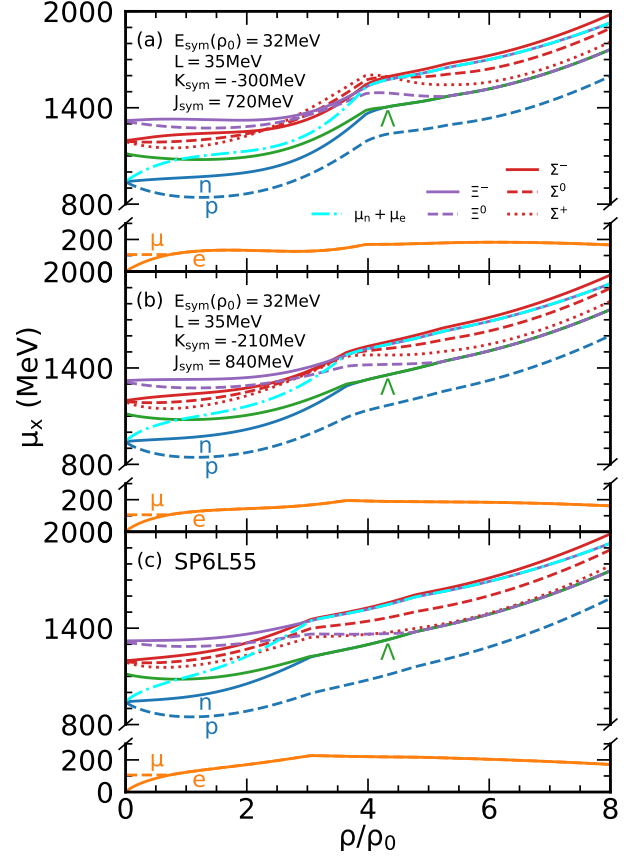


Figure 4. Particle chemical potentials in HS matter as a function of baryon density for the HSL35 interaction (a), the HSL35 but with $K_{\text{sym}} = -210 \text{ MeV}$ and $J_{\text{sym}} = 840 \text{ MeV}$ (b), and the SP6L55 interaction (c). The chemical potential sum $\mu_n + \mu_e$ for neutrons and electrons is also included.

It is instructive to have a further comprehensive understanding of the influence of K_{sym} and J_{sym} on properties of NSs and HSs. From Fig. 2 (e) - (h) and Fig. 3 (a), it is evident that a smaller value of K_{sym} combined with a smaller value of J_{sym} leads to a decrease in $E_{\text{sym}}(\rho)$ around $2 - 3\rho_0$. Consequently, the chemical potentials of neutrons in nuclear matter at these densities are reduced accordingly, making it hard for neutrons decaying into hyperons and thus pushing the hyperon appearance density to a higher value. On the other hand, beyond a density higher than about $4\rho_0$, there is an enhancement in $E_{\text{sym}}(\rho)$ which increases the neutron chemical potential and favors the appearance of hyperons. In other

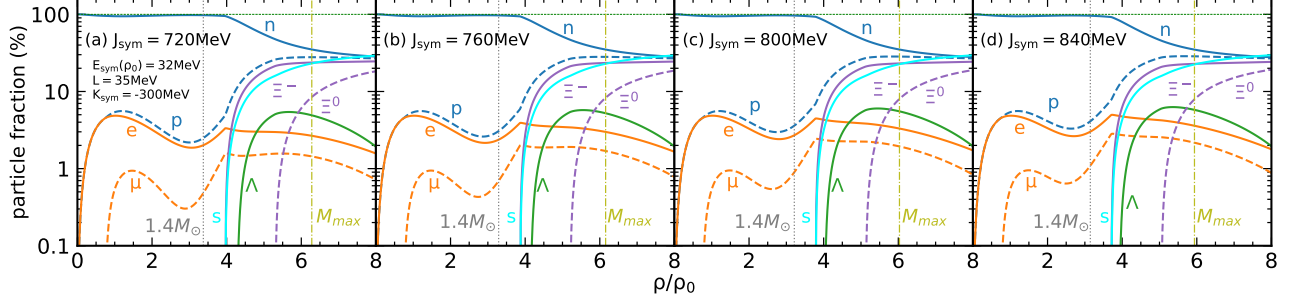


Figure 5. Particle fractions in HS matter as a function of baryon density for the HSL35 interaction but with $J_{\text{sym}} = 720$ MeV (a), 760 MeV (b), 800 MeV (c) and 840 MeV (d). Additionally, the central density for HSs with mass of $1.4M_{\odot}$ and maximum mass is indicated by the vertical lines, and the strangeness fraction denoted by “s” is also included.

words, having a soft density behavior for $E_{\text{sym}}(\rho)$ at densities between $2 - 3\rho_0$ but stiff above $4\rho_0$ can delay the critical emergence density for hyperons. This can be seen more clearly from Fig. 4 which shows the density dependence of particle chemical potentials in HS matter by varying individually K_{sym} and J_{sym} in the HSL35 interaction. For comparison, the corresponding results with SP6L55 are also included in Fig. 4. In particular, we note that the neutron chemical potential at $\rho = 2(3)\rho_0$ is 998(1107) MeV for $K_{\text{sym}} = -300$ MeV and $J_{\text{sym}} = 720$ MeV (a), 1017(1149) MeV for $K_{\text{sym}} = -210$ MeV and $J_{\text{sym}} = 840$ MeV (b), while it becomes 1054(1211) MeV for SP6L55 which comparatively has a much stiffer symmetry energy at intermediate density. Although both parameters K_{sym} and J_{sym} affect the critical emergence density of hyperons, their respective effects on the mass-radius relation and M_{TOV} are different due to their distinct impacts on the EOS for HS matter as reflected by the variations in the sound speed squared shown in the lowest row of Fig. 2. Therefore, the combined influence of K_{sym} and J_{sym} on the critical density for hyperon appearance and overall density behavior of HS matter EOS collectively shapes the properties of HSs.

Finally, we show in Fig. 5 the particle fraction and the strangeness fraction $\frac{\rho_s}{3\rho_B}$ in HS matter, by varying individually J_{sym} in HSL35. Here, ρ_s represents the total number density of constituent strange quarks within hadrons. Fig. 5 provides a clear depiction of the impact of J_{sym} on the critical emergence density of hyperons, i.e., a larger J_{sym} leads to a smaller critical emergence density of hyperons. In particular, Ξ^- appear first, then followed by Λ and last Ξ^0 as the density increases. The earlier appearance of Ξ^- is mainly because of the larger value of chemical potential sum $\mu_n + \mu_e$ for neutrons and electrons (see Fig. 4), which triggers the process $n + e^- \rightarrow \Xi^- + \nu_e$. In addition, it is seen from Fig. 5 that Σ hyperons do not appear at densities below $8\rho_0$ in the parameter space considered here, mainly due to their repulsive potentials which lead to large chemical poten-

tials for Σ hyperons as shown in Fig. 4. Furthermore, one can see clearly that the strangeness is not present for NSs with mass smaller than $1.4M_{\odot}$ and the strangeness fraction can reach to about 25% in the center of HSs with maximum mass configuration. Notably, it can be observed that the densities corresponding to the peaks (including the minor peaks) in C_s^2 for HS matter (as shown in the lowest row of Fig. 2) exactly coincide with the emergence densities of various types of hyperons.

4. CONCLUSION AND OUTLOOK

We have extended the nuclear N3LO Skyrme pseudopotential to include the interactions of octet baryons by assuming that the hyperon-nucleon and hyperon-hyperon interactions have similar density, momentum, and isospin dependence as for the nucleon-nucleon interaction. The parameters in these interactions are determined from either experimental information if any or microscopic calculations. By considering the constraints from microscopic calculations, terrestrial experiments and astrophysical observations, we have demonstrated that an appropriate high density behavior of the symmetry energy, namely, soft around $2 - 3\rho_0$ but stiff above about $4\rho_0$, offers a potential solution to the hyperon puzzle. The softening of the symmetry energy around $2 - 3\rho_0$ can effectively enhance the critical density for hyperon appearance in hyperon stars and thus mitigate the hyperon influence on properties of hyperon stars. In addition, the sound speed squared of the hyperon star matter exhibits a strong peak structure at density of $3 - 4\rho_0$ when the hyperons start to appear, providing a natural explanation on the similar phenomenon observed in the model-independent analysis on the multimessenger data.

In particular, our results indicate that the extended N3LO Skyrme pseudopotential HSL35 with a symmetry energy given by $E_{\text{sym}}(\rho_0) = 32$ MeV, slope parameter $L = 35$ MeV, curvature parameter $K_{\text{sym}} = -300$ MeV and skewness parameter $J_{\text{sym}} = 720$ MeV, which is soft around $2 - 3\rho_0$ but stiff above about $4\rho_0$, is able to

predict a maximum mass of $M_{\text{TOV}} \gtrsim 2M_{\odot}$ for static hyperon stars. At the same time, this extended N3LO Skyrme pseudopotential can be compatible with various constraints from theory, experiments and observations, including microscopic calculations on pure neutron matter, flow data in heavy-ion collisions, the tidal deformability $\Lambda_{1.4}$ from gravitational wave event GW170817, the observed mass-radius relation for compact stars from NICER as well as the unusually low mass and small radius in the central compact object of HESS J1731-347.

In future, it will be interesting to incorporate the extended N3LO Skyrme pseudopotential for the octet baryons in nuclear structure calculations and the transport model simulations for heavy-ion collisions. With the ongoing accumulation of more and more high quality data of hypernuclei as well as hyperon/hypernuclei production in heavy-ion collisions in terrestrial labora-

tories, more stringent constraints shall be obtained on the effective hyperon-nucleon and hyperon-hyperon interactions. These investigations will be useful to further address more precisely the hyperon puzzle as well as the hyperon roles on the dynamics of supernova explosions and binary neutron star mergers, and eventually to shed light on the QCD phase diagram of baryon-rich matter.

ACKNOWLEDGEMENTS

This work was supported in part by the National SKA Program of China (Grant No. 2020SKA0120300), the National Natural Science Foundation of China under Grant No 12235010, and the Science and Technology Commission of Shanghai Municipality (Grant No. 23JC1402700).

REFERENCES

- Abbott, B. P., et al. 2018, *Phys. Rev. Lett.*, 121, 161101, doi: [10.1103/PhysRevLett.121.161101](https://doi.org/10.1103/PhysRevLett.121.161101)
- Agrawal, B. K., De, J. N., & Samaddar, S. K. 2012, *Phys. Rev. Lett.*, 109, 262501, doi: [10.1103/PhysRevLett.109.262501](https://doi.org/10.1103/PhysRevLett.109.262501)
- Aichelin, J., & Ko, C. M. 1985, *Phys. Rev. Lett.*, 55, 2661, doi: [10.1103/PhysRevLett.55.2661](https://doi.org/10.1103/PhysRevLett.55.2661)
- Alexander, G., Karshon, U., Shapira, A., et al. 1968, *Phys. Rev.*, 173, 1452, doi: [10.1103/PhysRev.173.1452](https://doi.org/10.1103/PhysRev.173.1452)
- Antoniadis, J., et al. 2013, *Science*, 340, 6131, doi: [10.1126/science.1233232](https://doi.org/10.1126/science.1233232)
- Astashenok, A. V., Capozziello, S., & Odintsov, S. D. 2014, *Phys. Rev. D*, 89, 103509, doi: [10.1103/PhysRevD.89.103509](https://doi.org/10.1103/PhysRevD.89.103509)
- Baldo, M., Burgio, G. F., & Schulze, H. J. 2000, *Phys. Rev. C*, 61, 055801, doi: [10.1103/PhysRevC.61.055801](https://doi.org/10.1103/PhysRevC.61.055801)
- Baym, G., Pethick, C., & Sutherland, P. 1971, *Astrophys. J.*, 170, 299, doi: [10.1086/151216](https://doi.org/10.1086/151216)
- Beane, S. R., Chang, E., Cohen, S. D., et al. 2012, *Phys. Rev. Lett.*, 109, 172001, doi: [10.1103/PhysRevLett.109.172001](https://doi.org/10.1103/PhysRevLett.109.172001)
- Bednarek, I., Haensel, P., Zdunik, J. L., Bejger, M., & Manka, R. 2012, *Astron. Astrophys.*, 543, A157, doi: [10.1051/0004-6361/201118560](https://doi.org/10.1051/0004-6361/201118560)
- Bizarro, D., Rabhi, A., & Providência, C. 2015, <https://arxiv.org/abs/1502.04952>
- Bombaci, I. 2021, *Nucl. Phys. News*, 31, 17, doi: [10.1080/10619127.2021.1915024](https://doi.org/10.1080/10619127.2021.1915024)
- Brown, B. A. 2013, *Phys. Rev. Lett.*, 111, 232502, doi: [10.1103/PhysRevLett.111.232502](https://doi.org/10.1103/PhysRevLett.111.232502)
- Burgio, G. F., Schulze, H. J., Vidana, I., & Wei, J. B. 2021, *Prog. Part. Nucl. Phys.*, 120, 103879, doi: [10.1016/j.ppnp.2021.103879](https://doi.org/10.1016/j.ppnp.2021.103879)
- Cai, B.-J., & Chen, L.-W. 2012, *Phys. Lett. B*, 711, 104, doi: [10.1016/j.physletb.2012.03.058](https://doi.org/10.1016/j.physletb.2012.03.058)
- Cao, Z., & Chen, L.-W. 2023, <https://arxiv.org/abs/2308.16783>
- Carriere, J., Horowitz, C. J., & Piekarewicz, J. 2003, *Astrophys. J.*, 593, 463, doi: [10.1086/376515](https://doi.org/10.1086/376515)
- Cavagnoli, R., Menezes, D. P., & Providencia, C. 2011, *Phys. Rev. C*, 84, 065810, doi: [10.1103/PhysRevC.84.065810](https://doi.org/10.1103/PhysRevC.84.065810)
- Centelles, M., Roca-Maza, X., Vinas, X., & Warda, M. 2009, *Phys. Rev. Lett.*, 102, 122502, doi: [10.1103/PhysRevLett.102.122502](https://doi.org/10.1103/PhysRevLett.102.122502)
- Chatterjee, D., & Vidaña, I. 2016, *Eur. Phys. J. A*, 52, 29, doi: [10.1140/epja/i2016-16029-x](https://doi.org/10.1140/epja/i2016-16029-x)
- Chen, L.-W. 2011, *Sci. China Phys. Mech. Astron.*, 54, 124, doi: [10.1007/s11433-011-4415-9](https://doi.org/10.1007/s11433-011-4415-9)
- . 2015, *EPJ Web Conf.*, 88, 00017, doi: [10.1051/epjconf/20158800017](https://doi.org/10.1051/epjconf/20158800017)
- Chen, L.-W., Ko, C. M., & Li, B.-A. 2005a, *Phys. Rev. C*, 72, 064309, doi: [10.1103/PhysRevC.72.064309](https://doi.org/10.1103/PhysRevC.72.064309)
- . 2005b, *Phys. Rev. Lett.*, 94, 032701, doi: [10.1103/PhysRevLett.94.032701](https://doi.org/10.1103/PhysRevLett.94.032701)
- Chen, L.-W., Ko, C. M., Li, B.-A., & Xu, J. 2010, *Phys. Rev. C*, 82, 024321, doi: [10.1103/PhysRevC.82.024321](https://doi.org/10.1103/PhysRevC.82.024321)
- Chen, R., Cai, B.-J., Chen, L.-W., et al. 2012, *Phys. Rev. C*, 85, 024305, doi: [10.1103/PhysRevC.85.024305](https://doi.org/10.1103/PhysRevC.85.024305)
- Choi, S., Miyatsu, T., Cheoun, M.-K., & Saito, K. 2021, *Astrophys. J.*, 909, 156, doi: [10.3847/1538-4357/abe3fe](https://doi.org/10.3847/1538-4357/abe3fe)

- Chorozidou, A., & Gaitanos, T. 2024, *Phys. Rev. C*, 109, L032801, doi: [10.1103/PhysRevC.109.L032801](https://doi.org/10.1103/PhysRevC.109.L032801)
- Choudhury, D., et al. 2024, *Astrophys. J. Lett.*, 971, L20, doi: [10.3847/2041-8213/ad5a6f](https://doi.org/10.3847/2041-8213/ad5a6f)
- Cooper, E. D., Hama, S., Clark, B. C., & Mercer, R. L. 1993, *Phys. Rev. C*, 47, 297, doi: [10.1103/PhysRevC.47.297](https://doi.org/10.1103/PhysRevC.47.297)
- Cromartie, H. T., et al. 2019, *Nature Astron.*, 4, 72, doi: [10.1038/s41550-019-0880-2](https://doi.org/10.1038/s41550-019-0880-2)
- Danielewicz, P., Lacey, R., & Lynch, W. G. 2002, *Science*, 298, 1592, doi: [10.1126/science.1078070](https://doi.org/10.1126/science.1078070)
- Danielewicz, P., & Lee, J. 2014, *Nucl. Phys. A*, 922, 1, doi: [10.1016/j.nuclphysa.2013.11.005](https://doi.org/10.1016/j.nuclphysa.2013.11.005)
- Danielewicz, P., Singh, P., & Lee, J. 2017, *Nucl. Phys. A*, 958, 147, doi: [10.1016/j.nuclphysa.2016.11.008](https://doi.org/10.1016/j.nuclphysa.2016.11.008)
- Danyasz, M., et al. 1963, *Phys. Rev. Lett.*, 11, 29, doi: [10.1103/PhysRevLett.11.29](https://doi.org/10.1103/PhysRevLett.11.29)
- Das, C. B., Gupta, S. D., Gale, C., & Li, B.-A. 2003, *Phys. Rev. C*, 67, 034611, doi: [10.1103/PhysRevC.67.034611](https://doi.org/10.1103/PhysRevC.67.034611)
- Doroshenko, V., Suleimanov, V., Pühlhofer, G., & Santangelo, A. 2022, *Nature Astron.*, 6, 1444, doi: [10.1038/s41550-022-01800-1](https://doi.org/10.1038/s41550-022-01800-1)
- Drago, A., Lavagno, A., Pagliara, G., & Pigato, D. 2014, *Phys. Rev. C*, 90, 065809, doi: [10.1103/PhysRevC.90.065809](https://doi.org/10.1103/PhysRevC.90.065809)
- Eisele, F., Filthuth, H., Foehlich, W., Hepp, V., & Zech, G. 1971, *Phys. Lett. B*, 37, 204, doi: [10.1016/0370-2693\(71\)90053-0](https://doi.org/10.1016/0370-2693(71)90053-0)
- Engelmann, R., Filthuth, H., Hepp, V., & Kluge, E. 1966, *Phys. Lett.*, 21, 587, doi: [10.1016/0031-9163\(66\)91310-2](https://doi.org/10.1016/0031-9163(66)91310-2)
- Fiorella Burgio, G., & Fantina, A. F. 2018, *Astrophys. Space Sci. Libr.*, 457, 255, doi: [10.1007/978-3-319-97616-7_6](https://doi.org/10.1007/978-3-319-97616-7_6)
- Fonseca, E., et al. 2021, *Astrophys. J. Lett.*, 915, L12, doi: [10.3847/2041-8213/ac03b8](https://doi.org/10.3847/2041-8213/ac03b8)
- Friedman, E., & Gal, A. 2007, *Phys. Rept.*, 452, 89, doi: [10.1016/j.physrep.2007.08.002](https://doi.org/10.1016/j.physrep.2007.08.002)
- . 2021, *Phys. Lett. B*, 820, 136555, doi: [10.1016/j.physletb.2021.136555](https://doi.org/10.1016/j.physletb.2021.136555)
- Friedman, E., & Gal, A. 2024. <https://arxiv.org/abs/2411.11751>
- Fuchs, C. 2006, *Prog. Part. Nucl. Phys.*, 56, 1, doi: [10.1016/j.pnpnp.2005.07.004](https://doi.org/10.1016/j.pnpnp.2005.07.004)
- Fuchs, C., Faessler, A., Zabrodin, E., & Zheng, Y.-M. 2001, *Phys. Rev. Lett.*, 86, 1974, doi: [10.1103/PhysRevLett.86.1974](https://doi.org/10.1103/PhysRevLett.86.1974)
- Fujiwara, Y., Suzuki, Y., & Nakamoto, C. 2007, *Prog. Part. Nucl. Phys.*, 58, 439, doi: [10.1016/j.pnpnp.2006.08.001](https://doi.org/10.1016/j.pnpnp.2006.08.001)
- Garg, U., & Colò, G. 2018, *Prog. Part. Nucl. Phys.*, 101, 55, doi: [10.1016/j.pnpnp.2018.03.001](https://doi.org/10.1016/j.pnpnp.2018.03.001)
- Gerstung, D., Kaiser, N., & Weise, W. 2020, *Eur. Phys. J. A*, 56, 175, doi: [10.1140/epja/s10050-020-00180-2](https://doi.org/10.1140/epja/s10050-020-00180-2)
- Ghosh, S., Pradhan, B. K., Chatterjee, D., & Schaffner-Bielich, J. 2022, *Front. Astron. Space Sci.*, 9, 864294, doi: [10.3389/fspas.2022.864294](https://doi.org/10.3389/fspas.2022.864294)
- Glendenning, N. K., & Schaffner-Bielich, J. 1998, *Phys. Rev. Lett.*, 81, 4564, doi: [10.1103/PhysRevLett.81.4564](https://doi.org/10.1103/PhysRevLett.81.4564)
- Gomes, R. O., Dexheimer, V., Schramm, S., & Vasconcellos, C. A. Z. 2015, *Astrophys. J.*, 808, 8, doi: [10.1088/0004-637X/808/1/8](https://doi.org/10.1088/0004-637X/808/1/8)
- Haidenbauer, J., Petschauer, S., Kaiser, N., et al. 2013, *Nucl. Phys. A*, 915, 24, doi: [10.1016/j.nuclphysa.2013.06.008](https://doi.org/10.1016/j.nuclphysa.2013.06.008)
- Hama, S., Clark, B. C., Cooper, E. D., Sherif, H. S., & Mercer, R. L. 1990, *Phys. Rev. C*, 41, 2737, doi: [10.1103/PhysRevC.41.2737](https://doi.org/10.1103/PhysRevC.41.2737)
- Hartnack, C., Oeschler, H., & Aichelin, J. 2006, *Phys. Rev. Lett.*, 96, 012302, doi: [10.1103/PhysRevLett.96.012302](https://doi.org/10.1103/PhysRevLett.96.012302)
- Holzenkamp, B., Holinde, K., & Speth, J. 1989, *Nucl. Phys. A*, 500, 485, doi: [10.1016/0375-9474\(89\)90223-6](https://doi.org/10.1016/0375-9474(89)90223-6)
- Hugenholtz, N. M., & van Hove, L. 1958, *Physica*, 24, 363, doi: [10.1016/S0031-8914\(58\)95281-9](https://doi.org/10.1016/S0031-8914(58)95281-9)
- Huth, S., Wellenhofer, C., & Schwenk, A. 2021, *Phys. Rev. C*, 103, 025803, doi: [10.1103/PhysRevC.103.025803](https://doi.org/10.1103/PhysRevC.103.025803)
- Iida, K., & Sato, K. 1997, *Astrophys. J.*, 477, 294, doi: [10.1086/303685](https://doi.org/10.1086/303685)
- Inoue, T. 2019, *AIP Conf. Proc.*, 2130, 020002, doi: [10.1063/1.5118370](https://doi.org/10.1063/1.5118370)
- Ishii, N., Aoki, S., & Hatsuda, T. 2007, *Phys. Rev. Lett.*, 99, 022001, doi: [10.1103/PhysRevLett.99.022001](https://doi.org/10.1103/PhysRevLett.99.022001)
- Jiang, W.-Z., Li, B.-A., & Chen, L.-W. 2012, *Astrophys. J.*, 756, 56, doi: [10.1088/0004-637X/756/1/56](https://doi.org/10.1088/0004-637X/756/1/56)
- Kadyk, J. A., Alexander, G., Chan, J. H., Gaposchkin, P., & Trilling, G. H. 1971, *Nucl. Phys. B*, 27, 13, doi: [10.1016/0550-3213\(71\)90076-9](https://doi.org/10.1016/0550-3213(71)90076-9)
- Kochankovski, H., Ramos, A., & Tolos, L. 2024, *Mon. Not. Roy. Astron. Soc.*, 528, 2629, doi: [10.1093/mnras/stae231](https://doi.org/10.1093/mnras/stae231)
- Koehn, H., et al. 2024. <https://arxiv.org/abs/2402.04172>
- Kowalski, S., et al. 2007, *Phys. Rev. C*, 75, 014601, doi: [10.1103/PhysRevC.75.014601](https://doi.org/10.1103/PhysRevC.75.014601)
- Krastev, P. G. 2022, *Galaxies*, 10, 16, doi: [10.3390/galaxies10010016](https://doi.org/10.3390/galaxies10010016)
- Kumar, R., Aryal, K., Clevinger, A., & Dexheimer, V. 2024, *Phys. Lett. B*, 849, 138475, doi: [10.1016/j.physletb.2024.138475](https://doi.org/10.1016/j.physletb.2024.138475)
- Le Fèvre, A., Leifels, Y., Reisdorf, W., Aichelin, J., & Hartnack, C. 2016, *Nucl. Phys. A*, 945, 112, doi: [10.1016/j.nuclphysa.2015.09.015](https://doi.org/10.1016/j.nuclphysa.2015.09.015)
- Li, B.-A., Cai, B.-J., Xie, W.-J., & Zhang, N.-B. 2021, *Universe*, 7, 182, doi: [10.3390/universe7060182](https://doi.org/10.3390/universe7060182)

- Li, B.-A., & Chen, L.-W. 2005, *Phys. Rev. C*, 72, 064611, doi: [10.1103/PhysRevC.72.064611](https://doi.org/10.1103/PhysRevC.72.064611)
- Li, B.-A., Chen, L.-W., & Ko, C. M. 2008, *Phys. Rept.*, 464, 113, doi: [10.1016/j.physrep.2008.04.005](https://doi.org/10.1016/j.physrep.2008.04.005)
- Li, J. J., Long, W. H., & Sedrakian, A. 2018a, *Eur. Phys. J. A*, 54, 133, doi: [10.1140/epja/i2018-12566-6](https://doi.org/10.1140/epja/i2018-12566-6)
- Li, J. J., Sedrakian, A., & Weber, F. 2018b, *Phys. Lett. B*, 783, 234, doi: [10.1016/j.physletb.2018.06.051](https://doi.org/10.1016/j.physletb.2018.06.051)
- Li, T., et al. 2007, *Phys. Rev. Lett.*, 99, 162503, doi: [10.1103/PhysRevLett.99.162503](https://doi.org/10.1103/PhysRevLett.99.162503)
- Li, Z. H., & Schulze, H. J. 2008, *Phys. Rev. C*, 78, 028801, doi: [10.1103/PhysRevC.78.028801](https://doi.org/10.1103/PhysRevC.78.028801)
- Li, Z. Z., Niu, Y. F., & Colò, G. 2023, *Phys. Rev. Lett.*, 131, 082501, doi: [10.1103/PhysRevLett.131.082501](https://doi.org/10.1103/PhysRevLett.131.082501)
- Logoteta, D., Vidana, I., & Bombaci, I. 2019, *Eur. Phys. J. A*, 55, 207, doi: [10.1140/epja/i2019-12909-9](https://doi.org/10.1140/epja/i2019-12909-9)
- Lonardoni, D., Lovato, A., Gandolfi, S., & Pederiva, F. 2015, *Phys. Rev. Lett.*, 114, 092301, doi: [10.1103/PhysRevLett.114.092301](https://doi.org/10.1103/PhysRevLett.114.092301)
- Maslov, K. A., Kolomeitsev, E. E., & Voskresensky, D. N. 2015, *Phys. Lett. B*, 748, 369, doi: [10.1016/j.physletb.2015.07.032](https://doi.org/10.1016/j.physletb.2015.07.032)
- Millener, D. J., Dover, C. B., & Gal, A. 1988, *Phys. Rev. C*, 38, 2700, doi: [10.1103/PhysRevC.38.2700](https://doi.org/10.1103/PhysRevC.38.2700)
- Miller, M. C., et al. 2019, *Astrophys. J. Lett.*, 887, L24, doi: [10.3847/2041-8213/ab50c5](https://doi.org/10.3847/2041-8213/ab50c5)
- . 2021, *Astrophys. J. Lett.*, 918, L28, doi: [10.3847/2041-8213/ac089b](https://doi.org/10.3847/2041-8213/ac089b)
- Morfouace, P., et al. 2019, *Phys. Lett. B*, 799, 135045, doi: [10.1016/j.physletb.2019.135045](https://doi.org/10.1016/j.physletb.2019.135045)
- Muto, T. 2008, *Phys. Rev. C*, 77, 015810, doi: [10.1103/PhysRevC.77.015810](https://doi.org/10.1103/PhysRevC.77.015810)
- Nemura, H., et al. 2018, *EPJ Web Conf.*, 175, 05030, doi: [10.1051/epjconf/201817505030](https://doi.org/10.1051/epjconf/201817505030)
- Ozel, F., Psaltis, D., Ransom, S., Demorest, P., & Alford, M. 2010, *Astrophys. J. Lett.*, 724, L199, doi: [10.1088/2041-8205/724/2/L199](https://doi.org/10.1088/2041-8205/724/2/L199)
- Petschauer, S., Haidenbauer, J., Kaiser, N., Meißner, U.-G., & Weise, W. 2016, *Eur. Phys. J. A*, 52, 15, doi: [10.1140/epja/i2016-16015-4](https://doi.org/10.1140/epja/i2016-16015-4)
- Polinder, H., Haidenbauer, J., & Meißner, U.-G. 2006, *Nucl. Phys. A*, 779, 244, doi: [10.1016/j.nuclphysa.2006.09.006](https://doi.org/10.1016/j.nuclphysa.2006.09.006)
- Providência, C., Fortin, M., Pais, H., & Rabhi, A. 2018, doi: [10.3389/fspas.2019.00013](https://doi.org/10.3389/fspas.2019.00013)
- Providencia, C., & Rabhi, A. 2013, *Phys. Rev. C*, 87, 055801, doi: [10.1103/PhysRevC.87.055801](https://doi.org/10.1103/PhysRevC.87.055801)
- Providência, C., Avancini, S. S., Cavagnoli, R., et al. 2014, *Eur. Phys. J. A*, 50, 44, doi: [10.1140/epja/i2014-14044-7](https://doi.org/10.1140/epja/i2014-14044-7)
- Prowse, D. J. 1966, *Phys. Rev. Lett.*, 17, 782, doi: [10.1103/PhysRevLett.17.782](https://doi.org/10.1103/PhysRevLett.17.782)
- Qiu, M., Cai, B.-J., Chen, L.-W., Yuan, C.-X., & Zhang, Z. 2024, *Phys. Lett. B*, 849, 138435, doi: [10.1016/j.physletb.2023.138435](https://doi.org/10.1016/j.physletb.2023.138435)
- Rijken, T. A., Stoks, V. G. J., & Yamamoto, Y. 1999, *Phys. Rev. C*, 59, 21, doi: [10.1103/PhysRevC.59.21](https://doi.org/10.1103/PhysRevC.59.21)
- Riley, T. E., et al. 2019, *Astrophys. J. Lett.*, 887, L21, doi: [10.3847/2041-8213/ab481c](https://doi.org/10.3847/2041-8213/ab481c)
- . 2021, *Astrophys. J. Lett.*, 918, L27, doi: [10.3847/2041-8213/ac0a81](https://doi.org/10.3847/2041-8213/ac0a81)
- Roca-Maza, X., Brenna, M., Agrawal, B. K., et al. 2013, *Phys. Rev. C*, 87, 034301, doi: [10.1103/PhysRevC.87.034301](https://doi.org/10.1103/PhysRevC.87.034301)
- Ryu, C.-Y., Hyun, C. H., & Lee, C.-H. 2011, *Phys. Rev. C*, 84, 035809, doi: [10.1103/PhysRevC.84.035809](https://doi.org/10.1103/PhysRevC.84.035809)
- Satpathy, L., Maheswari, V., & Nayak, R. 1999, *Physics Reports*, 319, 85, doi: [https://doi.org/10.1016/S0370-1573\(99\)00011-3](https://doi.org/https://doi.org/10.1016/S0370-1573(99)00011-3)
- Schaffner, J., Dover, C. B., Gal, A., et al. 1994, *Annals Phys.*, 235, 35, doi: [10.1006/aphy.1994.1090](https://doi.org/10.1006/aphy.1994.1090)
- Sechi-Zorn, B., Kehoe, B., Twitty, J., & Burnstein, R. A. 1968, *Phys. Rev.*, 175, 1735, doi: [10.1103/PhysRev.175.1735](https://doi.org/10.1103/PhysRev.175.1735)
- Serot, B. D., & Walecka, J. D. 1997, *Int. J. Mod. Phys. E*, 6, 515, doi: [10.1142/S0218301397000299](https://doi.org/10.1142/S0218301397000299)
- Shetty, D. V., Yennello, S. J., & Souliotis, G. A. 2007, *Phys. Rev. C*, 75, 034602, doi: [10.1103/PhysRevC.75.034602](https://doi.org/10.1103/PhysRevC.75.034602)
- Shlomo, S., Kolomietz, V. M., & Colò, G. 2006, *Eur. Phys. J. A*, 30, 23, doi: [10.1140/epja/i2006-10100-3](https://doi.org/10.1140/epja/i2006-10100-3)
- Skyrme, T. 1959, *Nucl. Phys.*, 9, 615, doi: [10.1016/0029-5582\(58\)90345-6](https://doi.org/10.1016/0029-5582(58)90345-6)
- Sorensen, A., et al. 2024, *Prog. Part. Nucl. Phys.*, 134, 104080, doi: [10.1016/j.ppnp.2023.104080](https://doi.org/10.1016/j.ppnp.2023.104080)
- Stoks, V. G. J., & Rijken, T. A. 1999, *Phys. Rev. C*, 59, 3009, doi: [10.1103/PhysRevC.59.3009](https://doi.org/10.1103/PhysRevC.59.3009)
- Sun, X., Miao, Z., Sun, B., & Li, A. 2023, *Astrophys. J.*, 942, 55, doi: [10.3847/1538-4357/ac9d9a](https://doi.org/10.3847/1538-4357/ac9d9a)
- Takahashi, H., et al. 2001, *Phys. Rev. Lett.*, 87, 212502, doi: [10.1103/PhysRevLett.87.212502](https://doi.org/10.1103/PhysRevLett.87.212502)
- Thapa, V. B., & Sinha, M. 2022, *Phys. Rev. C*, 105, 015802, doi: [10.1103/PhysRevC.105.015802](https://doi.org/10.1103/PhysRevC.105.015802)
- Tolos, L. 2024, *Acta Phys. Polon. B*, 55, 5, doi: [10.5506/APhysPolB.55.5-A1](https://doi.org/10.5506/APhysPolB.55.5-A1)
- Tolos, L., & Fabbietti, L. 2020, *Prog. Part. Nucl. Phys.*, 112, 103770, doi: [10.1016/j.ppnp.2020.103770](https://doi.org/10.1016/j.ppnp.2020.103770)
- Tsang, M. B., Zhang, Y., Danielewicz, P., et al. 2009, *Phys. Rev. Lett.*, 102, 122701, doi: [10.1103/PhysRevLett.102.122701](https://doi.org/10.1103/PhysRevLett.102.122701)

- Tsubakihara, K., & Ohnishi, A. 2013, Nucl. Phys. A, 914, 438, doi: [10.1016/j.nuclphysa.2013.04.006](https://doi.org/10.1016/j.nuclphysa.2013.04.006)
- Vidaña, I. 2018, Proc. Roy. Soc. Lond. A, 474, 0145, doi: [10.1098/rspa.2018.0145](https://doi.org/10.1098/rspa.2018.0145)
- . 2022, EPJ Web Conf., 271, 09001, doi: [10.1051/epjconf/202227109001](https://doi.org/10.1051/epjconf/202227109001)
- Vidana, I., Polls, A., Ramos, A., Engvik, L., & Hjorth-Jensen, M. 2000, Phys. Rev. C, 62, 035801, doi: [10.1103/PhysRevC.62.035801](https://doi.org/10.1103/PhysRevC.62.035801)
- Wada, R., et al. 2012, Phys. Rev. C, 85, 064618, doi: [10.1103/PhysRevC.85.064618](https://doi.org/10.1103/PhysRevC.85.064618)
- Walecka, J. D. 1985, ADVANCES IN NUCLEAR PHYSICS
- Wang, R., Chen, L.-W., & Zhou, Y. 2018, Phys. Rev. C, 98, 054618, doi: [10.1103/PhysRevC.98.054618](https://doi.org/10.1103/PhysRevC.98.054618)
- Wang, S.-P., Wang, R., Ye, J.-T., & Chen, L.-W. 2024, Phys. Rev. C, 109, 054623, doi: [10.1103/PhysRevC.109.054623](https://doi.org/10.1103/PhysRevC.109.054623)
- Wei, S.-N., Feng, Z.-Q., & Jiang, W.-Z. 2024, Phys. Lett. B, 853, 138658, doi: [10.1016/j.physletb.2024.138658](https://doi.org/10.1016/j.physletb.2024.138658)
- Weinberg, S. 1990, Phys. Lett. B, 251, 288, doi: [10.1016/0370-2693\(90\)90938-3](https://doi.org/10.1016/0370-2693(90)90938-3)
- Weissenborn, S., Chatterjee, D., & Schaffner-Bielich, J. 2012, Phys. Rev. C, 85, 065802, doi: [10.1103/PhysRevC.85.065802](https://doi.org/10.1103/PhysRevC.85.065802)
- Weissenborn, S., Sagert, I., Pagliara, G., Hempel, M., & Schaffner-Bielich, J. 2011, Astrophys. J. Lett., 740, L14, doi: [10.1088/2041-8205/740/1/L14](https://doi.org/10.1088/2041-8205/740/1/L14)
- Xu, C., Li, B.-A., & Chen, L.-W. 2010a, Phys. Rev. C, 82, 054607, doi: [10.1103/PhysRevC.82.054607](https://doi.org/10.1103/PhysRevC.82.054607)
- Xu, J., Chen, L.-W., Ko, C. M., & Li, B.-A. 2010b, Phys. Rev. C, 81, 055803, doi: [10.1103/PhysRevC.81.055803](https://doi.org/10.1103/PhysRevC.81.055803)
- Xu, J., Chen, L.-W., Li, B.-A., & Ma, H.-R. 2009a, Astrophys. J., 697, 1549, doi: [10.1088/0004-637X/697/2/1549](https://doi.org/10.1088/0004-637X/697/2/1549)
- . 2009b, Phys. Rev. C, 79, 035802, doi: [10.1103/PhysRevC.79.035802](https://doi.org/10.1103/PhysRevC.79.035802)
- Xu, J., Zhou, J., Zhang, Z., Xie, W.-J., & Li, B.-A. 2020, Phys. Lett. B, 810, 135820, doi: [10.1016/j.physletb.2020.135820](https://doi.org/10.1016/j.physletb.2020.135820)
- Youngblood, D. H., Clark, H. L., & Lui, Y. W. 1999, Phys. Rev. Lett., 82, 691, doi: [10.1103/PhysRevLett.82.691](https://doi.org/10.1103/PhysRevLett.82.691)
- Yue, T.-G., Chen, L.-W., Zhang, Z., & Zhou, Y. 2022, Phys. Rev. Res., 4, L022054, doi: [10.1103/PhysRevResearch.4.L022054](https://doi.org/10.1103/PhysRevResearch.4.L022054)
- Zdunik, J. L., & Haensel, P. 2013, Astron. Astrophys., 551, A61, doi: [10.1051/0004-6361/201220697](https://doi.org/10.1051/0004-6361/201220697)
- Zhang, N.-B., & Li, B.-A. 2019, Eur. Phys. J. A, 55, 39, doi: [10.1140/epja/i2019-12700-0](https://doi.org/10.1140/epja/i2019-12700-0)
- Zhang, Y., Liu, M., Xia, C.-J., Li, Z., & Biswal, S. K. 2020, Phys. Rev. C, 101, 034303, doi: [10.1103/PhysRevC.101.034303](https://doi.org/10.1103/PhysRevC.101.034303)
- Zhang, Z., & Chen, L.-W. 2013, Phys. Lett. B, 726, 234, doi: [10.1016/j.physletb.2013.08.002](https://doi.org/10.1016/j.physletb.2013.08.002)
- . 2014, Phys. Rev. C, 90, 064317, doi: [10.1103/PhysRevC.90.064317](https://doi.org/10.1103/PhysRevC.90.064317)
- . 2019, Phys. Rev. C, 100, 044301, doi: [10.1103/PhysRevC.100.044301](https://doi.org/10.1103/PhysRevC.100.044301)
- . 2023, Phys. Rev. C, 108, 024317, doi: [10.1103/PhysRevC.108.024317](https://doi.org/10.1103/PhysRevC.108.024317)
- Zhou, Y., & Chen, L.-W. 2019, Astrophys. J., 886, 52, doi: [10.3847/1538-4357/ab4adf](https://doi.org/10.3847/1538-4357/ab4adf)
- Zhou, Y., Chen, L.-W., & Zhang, Z. 2019, Phys. Rev. D, 99, 121301, doi: [10.1103/PhysRevD.99.121301](https://doi.org/10.1103/PhysRevD.99.121301)